Environmental Research 239 (2023) 117115

Contents lists available at ScienceDirect

Environmental Research

journal homepage: www.elsevier.com/locate/envres

Application of lipid and polymeric-based nanoparticles for treatment of inner ear infections via XGBoost

Jie Zhang [a,1], Ru Chen [b,1], Shuainan Chen [a,1], Die Yu [a,1], Dalia H. Elkamchouchi [c], Mohammed S. Alqahtani [d,e], Hamid Assilzadeh [f,g,h,i,***], Zhongguan Huang [j,*], Yideng Huang [a,**]

[a] Department of Otolaryngology, The First Affiliated Hospital of Wenzhou Medical University, Wenzhou, Zhejiang,325000, China
[b] Department of Otolaryngology, The Third Affiliated Hospital of Wenzhou Medical University, Wenzhou, Zhejiang 325000, China
[c] Department of Information Technology, College of Computer and Information Sciences, Princess Nourah bint Abdulrahman University, P.O. Box 84428, Riyadh 11671, Saudi Arabia
[d] Radiological Sciences Department, College of Applied Medical Sciences, King Khalid University, Abha 61421, Saudi Arabia
[e] BioImaging Unit, Space Research Centre, Michael Atiyah Building, University of Leicester, Leicester, LE1 7RH, UK
[f] Faculty of Architecture and Urbanism, UTE University, Calle Rumipamba S/N and Bourgeois, Quito, Ecuador
[g] Institute of Research and Development, Duy Tan University, Da Nang, Viet Nam
[h] School of Engineering & Technology, Duy Tan University, Da Nang, Viet Nam
[i] Department of Biomaterials, Saveetha Dental College and Hospital, Saveetha Institute of Medical and Technical Sciences, Chennai 600077, India
[j] Department of Otolaryngology, Pingyang Affiliated Hospital of Wenzhou Medical University, Pingyang, Zhejiang, 325400, China

ARTICLE INFO

Keywords:
Chronic otitis media (COM)
Zinc oxide
Smart nanotechnology
Otitis media with effusion (OME)
Wideband absorbance immittance (WAI)
XGBoost

ABSTRACT

Taking hearing loss as a prevalent sensory disorder, the restricted permeability of blood flow and the blood-labyrinth barrier in the inner ear pose significant challenges to transporting drugs to the inner ear tissues. The current options for hear loss consist of cochlear surgery, medication, and hearing devices. There are some restrictions to the conventional drug delivery methods to treat inner ear illnesses, however, different smart nanoparticles, including inorganic-based nanoparticles, have been presented to regulate drug administration, enhance the targeting of particular cells, and decrease systemic adverse effects. Zinc oxide nanoparticles possess distinct characteristics that facilitate accurate drug delivery, improved targeting of specific cells, and minimized systemic adverse effects. Zinc oxide nanoparticles was studied for targeted delivery and controlled release of therapeutic drugs within specific cells. XGBoost model is used on the Wideband Absorbance Immittance (WAI) measuring test after cochlear surgery. There were 90 middle ear effusion samples (ages = 1–10 years, mean = 34.9 months) had chronic middle ear effusion for four months and verified effusion for seven weeks. In this research, 400 sets underwent wideband absorbance imaging (WAI) to assess inner ear performance after surgery. Among them, 60 patients had effusion Otitis Media with Effusion (OME), while 30 ones had normal ears (control). OME ears showed significantly lower absorbance at 250, 500, and 1000 Hz than controls ($p < 0.001$). Absorbance thresholds >0.252 (1000 Hz) and >0.330 (2000 Hz) predicted a favorable prognosis ($p < 0.05$, odds ratio: 6). It means that cochlear surgery and WAI showed high function in diagnosis and treatment of inner ear infections. Regarding the R^2 0.899 and RMSE 1.223, XGBoost shows excellent specificity and sensitivity for categorizing ears as having effusions absent or present or partial or complete flows present, with areas under the curve (1–0.944).

1. Introduction

Hearing impairment is a common condition caused by sensory loss, substantially impacting human health and overall well-being. According to a study by the World Health Organization (WHO) 2005, the prevalence of hearing loss was estimated to affect more than 250 million

* Corresponding author.
** Corresponding author.
*** Corresponding author.
E-mail addresses: hamidassilzadeh@duytan.edu.vn (H. Assilzadeh), zghuang73@Hotmail.com (Z. Huang), huangyideng@wmu.edu.cn (Y. Huang).
[1] These authors contributed to this work equally.

https://doi.org/10.1016/j.envres.2023.117115
Received 18 July 2023; Received in revised form 26 August 2023; Accepted 9 September 2023
Available online 16 September 2023

individuals worldwide. By 2050, about 5% of the global population will suffer hearing loss. The outer ear begins the process of hearing by collecting sound waves (Praetorius et al., 2007; Ross et al., 2016; Schilder et al., 2019). Injections of liquid medications into the tympanic membrane are the most commonly used treatment for the inner ear. Additional delivery technologies exist, including nanocarrier delivery systems and hydrogel delivery systems. Fig. 1 depicts a schematic we you of the ear, illustrating its various sections.

Treating inner ear problems presents challenges because of the intricate physiology and anatomy of the inner-ear. The blood-labyrinth barrier restricts drug access, leading to suboptimal drug concentrations and decreased treatment efficacy. The small size of inner ear and delicate components pose difficulties in delivering drugs precisely to target cells. Moreover, maintaining drug stability in the inner ear's dynamic environment adds complexity. Invasive treatments and limited accessibility demand innovative drug delivery methods. Systemic drug administration might not achieve sufficient drug levels, necessitating customized drug distribution to specific inner ear regions. Almost $3 billion was spent 1995 on acute otitis media-related treatment and missed school or work time. By this time, more than eighty percent of kids have been diagnosed with acute otitis media, the most prevalent form of the disease, which typically strikes among six and twenty-four months of age. In the absence of acute infection, middle-ear fluid is called OME (Klein et al.). After clearing up the disease, the effusion might linger for a while. Flow in the middle ear may occur after acute otitis media, or it can develop independently due to Eustachian tube dysfunction.

1.1. Smart nanoparticle-mediated therapies for inner ear infections

Penicillin-resistant Chronic and recurrent acute otitis media almost always results from infection with Streptococcus pneumoniae (Arrieta et al., 2004). Common nonspecific symptoms observed in infants and young children with (AOM) include headache, fever, cough, irritability, listlessness, rhinitis, anorexia, vomiting, diarrhea, and pressing at the ears. Otalgia is highest among individuals aged 12 and older, while it is less common among toddlers and infants (Klein et al.). Acute otitis media is frequently misidentified as an upper respiratory tract infection, and relying solely on symptoms is insufficient for accurate differentiation (Rothman et al., 2003). The presence of otalgia (ear pain), rubbing or dragging on the ear, and parental suspicion of otitis media are all considered positive symptoms with likelihood ratios (LR+) of 3.0 or higher. These symptoms significantly contribute to establishing a definitive diagnosis (Kontiokari et al., 1998; Niemela et al., 1994). Many people all over the globe suffer from inner ear problems, with deafness being the most frequent sensory impairment (Danti et al., 2020; Nguyen et al., 2017; Ren et al., 2019). Sensorineural hearing loss (SNHL), caused by problems in the cochlea, accounts for a significant portion of this problem. Inner ear infections, both congenital and acquired, have been implicated in causing some of these problem. Therefore, the high incidence of ear problems provides a strong motivation and an excellent chance to advance treatment strategies (Zhang et al., 2021a; McCall et al., 2010). In particular, the inner ear's tiny size, restricted accessibility, and high fragility limit available therapy choices (Mä et al., 2018). Distribution modalities now in use, such as intratympanic injection, systemic delivery, and direct inner ear medication delivery, all have drawbacks regarding effectiveness and invasiveness. There are two potential pathways by which the inflammation develops. Although the prevailing belief is that the latter is primarily attributed to a viral infection. However, this condition can only be applied if there is exclusive involvement of the vestibular branch of the eighth cranial nerve. Fig. 2 shows the inner ear surgery. Inner ear surgery, also known as otologic surgery, is a medical procedure performed to address issues within the inner ear, such as hearing loss, balance problems, or certain forms of tinnitus. Surgeons access the inner ear through the ear canal or behind the ear, using specialized techniques and equipment to repair or replace damaged structures like the cochlea or semicircular canals, aiming to improve hearing and balance function. This intricate procedure requires precision and expertise due to the delicate nature of the inner ear's components.

In a study, the researchers aimed to address the rapid evaporation of fragrances in aromatic products, shortening their useful life. They synthesized zwitterionic comb-like lipid polymers designed to encapsulate the fragrance molecule linalool to achieve this (Shu et al., 2021). The study's pivotal findings underscore the efficacy of zwitterionic comb-like lipid polymers as encapsulating agents for fragrances. Their

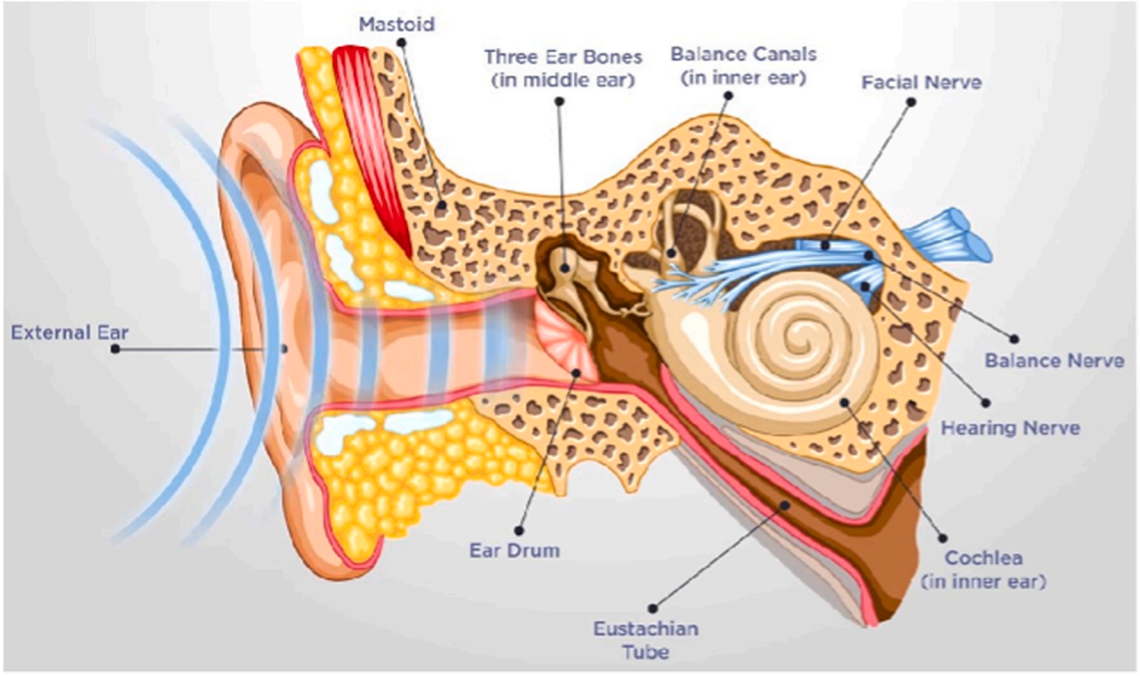

Fig. 1. Schematic view of the ear [Source by authors].

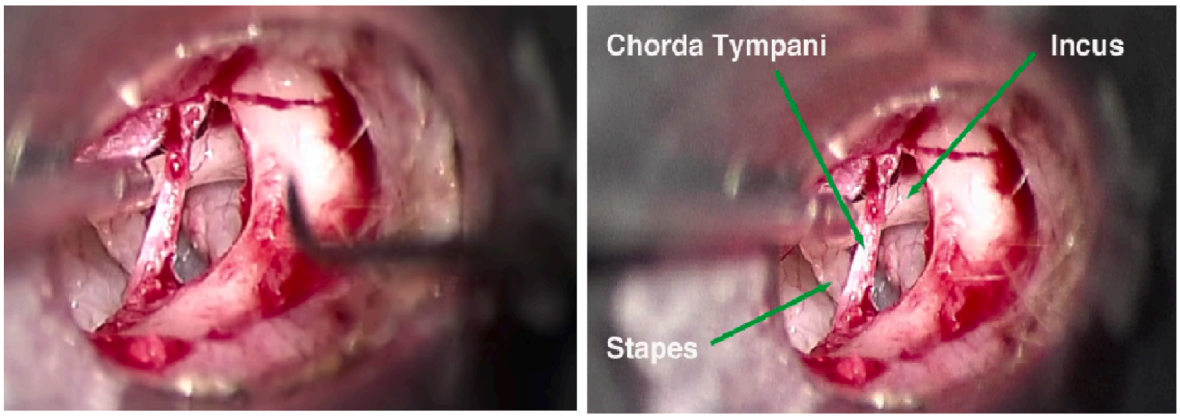

Fig. 2. Medical Intervention: Visualizing the Ear Drum and Fluid Accumulation. The subsequent steps involve a precise procedure to safely drain the fluid, providing relief and restoring auditory function [Source by authors].

superior capacity for encapsulation compared to linear lipid molecules not only ensures effective trapping and storage of fragrant compounds like linalool within nano-fragrances but also provides a platform for modulating the release rate. This controlled release mechanism is crucial in extending the fragrance retention period within aromatic products. By leveraging these properties, the study's approach offers a promising solution to counteract fragrance evaporation and prolong the lifespan of scented products. This scientific breakthrough not only addresses a longstanding challenge but also holds significant potential in revolutionizing the aromatic product industry by enhancing consumer satisfaction through prolonged fragrance enjoyment (Shu et al., 2021).

1.2. Literature review

In a research study, scientists devised an innovative method of administering protein-based medications by employing bifunctional oral lipid polymer hybrid nanoparticles referred to as R8-PEG-PPNPs. The purpose of this system was to address the challenge of maintaining the activity of protein-based drugs during oral delivery, which has limited their application in the past. The specific protein-based drug used in this study was superoxide dismutase (SOD), and the target condition for treatment was ulcerative colitis (UC) (Cui et al., 2022). The study's significant features and findings encompass the formulation and attributes of R8-PEG-PPNPs, which encompassed PCADK, PLGA, lecithin, stearic acid-octa-arginine, and PEG. The resulting nanoparticles demonstrated homogeneous distribution, spherical morphology, and structural integrity—qualities crucial for stable drug delivery. The success of R8-PEG-PPNPs lies in sustaining protein drug activity during oral delivery, showcasing biocompatibility, facilitating cellular uptake, and precision targeting to inflammation sites (Cui et al., 2022). Nanotechnology-driven targeted therapy, particularly using carbohydrate polymer-based nanocomposites, shows promise in treating breast cancer effectively while sparing normal cells due to their natural abundance, biocompatibility, and favorable properties. Another study highlighted the physicochemical attributes, biological effects, fabrication techniques, and potential of carbohydrate polymer-derived nanocomposites for breast cancer treatment and future prospects (Moghaddam et al., 2022). In another study, the authors devised a methodology to monitor the temperature of cancer cells following photothermal therapy, a critical factor in determining the treatment's efficacy. The existing techniques for measuring intracellular temperatures have certain limitations regarding their accuracy and spatial resolution, consequently restricting their practicality in photothermal therapy. The study focuses on a novel approach to monitor temperature during photothermal therapy using a system combining fluorescent polymers and modified gold nano bipyramids (AuNBPs). The system employs a mucin-1 protein aptamer for targeted recognition of cancer cells, reducing interference. AuNBPs' photothermal effect raises fluorescence intensity upon laser exposure, serving as a measurable temperature-sensing signal. Monitoring intracellular temperature changes in real time, the method offers an effective way to optimize photothermal therapy outcomes (Qiao et al., 2022).

The research paper presents a new and effective method for identifying nucleic acids within living cells. This method involves the utilization of a two-dimensional coordination polymer (CP) nanosheet known as [Cu(tz)] (Htz = 1,2,4-triazole). The nanosheet is synthesized using a straightforward bottom-up approach, which offers cost-effectiveness and time-efficiency advantages compared to currently available fluorescence biosensors based on nanomaterials (Xu et al., 2022).

In another study, researchers developed an ultrasensitive biosensor using Pt–Pd–ZnO/SWCNTs nanocomposites and ds-DNA to monitor the concentration of the anticancer drug idarubicin. The nanocomposite's structure was analyzed using microscopy techniques, and a layer-by-layer method was used to create the biosensor. This biosensor effectively detected idarubicin in biological fluids and pharmaceuticals, showing a detection range of 1.0 nM–65 μM and a low limit of 0.8 nM. Real sample testing demonstrated recovery rates of 98.0%–104.75%. Molecular docking confirmed the binding mode of idarubicin with ds-DNA. The study presents a promising approach for highly sensitive DNA biosensors in anticancer drug monitoring, combining nanocomposites and molecular docking insights (Karimi-Maleh et al., 2022).

In a study, researchers developed a sensitive DNA biosensor using ZIF-8/Co/rGO/C3N4 nanohybrid on a screen-printed carbon electrode to detect the herbicide Pendimethalin (PND) in real samples. The biosensor successfully quantified PND in concentrations from 0.01 to 35 μM, with a low detection limit of 8.0 nM. Real sample testing, including rice, wheat, tap, and river water, demonstrated a recovery range of 98.2–105.6%. Molecular docking analysis supported the biosensor's effectiveness in interacting with PND, paving the way for sensitive herbicide monitoring using nanohybrid-based biosensors (Karimi-Maleh et al., 2023).

Researchers introduced an innovative approach for precise nucleic acid quantification within viable cells. [Cu(tz)] nanosheets act as a versatile platform, assembling DNA probes and HCR probes for targeted detection and amplification. Achieving an ultrathin thickness of 4.7 ± 1.1 nm, these nano sensors exhibit remarkable sensitivity, with a LOD of 144 pmol/L for p53 DNA and 100 pmol/L for miR-21 in living cells. The method's reliability is confirmed by consistent results with qRT-PCR analysis. Notably, these nanosheets also exhibit potential for nucleic acid delivery, amplifying their role as a multifunctional platform in biomedical applications (Xu et al., 2022).

The research paper introduces a novel technique for detecting trace levels of uranyl ions in potable water, crucial for public safety and

environmental monitoring due to their radioactivity and toxicity. Utilizing electrochemiluminescence (ECL) imaging technology, scientists create three-in-one polymer nanoparticles (PNPs) modified with amidoxime. These PNPs exhibit ultra-low detection limits (0.5 ng/L), high selectivity, and visualized warning capabilities. Resonance energy transfer enhances ECL signals through uranyl ion participation. ECL imaging facilitates real-time, accurate detection in natural water samples, showcasing its potential for environmental monitoring and safeguarding water quality (Wang et al., 2022). The challenge in aromatic products is their short fragrance lifespan due to rapid evaporation. Researchers addressed this by creating zwitterionic comb-like lipid polymers to encase linalool scent. These polymers were more effective than linear lipids, enhancing linalool retention and slowing its release for longer-lasting nano-fragrance (Zhang et al., 2021b). Nanocomposites are solid materials with multiple phases (100 nm) (Buehler et al., 2019; Rasouli et al., 2023) and are classified as ceramic, polymer, and metal, according to Omanović-Mikličanin et al. (Omanović-Miklič et al., 2020). Metallic nanocomposites (MNCs) are fabricated by amalgamating two or more metallic elements (Basavegowda et al., 2020) (Buehler et al., 2019; Joo et al., 2020), while being examined in electronics, catalysis, chemistry, physics, and medicine (Buehler et al., 2019; Li et al., 2023). Cui et al. (2019) has established a wide notion that smaller multinational corporations (MNCs) exhibit greater strength or competitiveness in various aspects. Including medicine, absorbent materials, electronics, catalysis, optoelectronics, and catalysis (Cui et al., 2019; Basavegowda et al., 2020; Csarnovics et al., 2020; Heydari and Shariati, 2018; Sajedi and Shariati, 2019; Tavakkoli et al., 2022).

Pndimethalin (PND) is a chemical compound classified as a pre-emergence herbicide. Its primary purpose is to effectively manage the growth of grass and broadleaf weeds in various crops. The technology includes the inhibition of cell division in the root meristem, thereby preventing the growth of weed seedlings (Lee et al., 2022). It is frequently utilized with other herbicides to achieve a broader range of weed control (Shahnazi et al., 2020). Additionally, it is employed in non-agricultural contexts, such as the management of turf and landscaping (Cech et al., 2022). The chemical compound suppresses mitotic activity in the developing seedlings of undesirable plant species, thereby impeding their growth and development (Rohit et al., 2017).

Cancer has been widely recognized as a significant global issue, resulting in the loss of millions of lives over an extended time (Trichopoulos et al., 1972; Traverso et al., 2013; Sun et al., 2019) while using different drugs with distinct properties (Kirschner et al., 1997). However, the adverse impact of anticancer medications, which can have significant consequences, have traditionally been recognized as a limiting factor in the efficacy of treatment (Vigano et al., 2018). Nevertheless, the significant challenges to address in the detection of drug compounds using electrochemical sensors are the elevated overpotential and diminished redox current (Ensafi et al., 2011; Öet al., 2020; Karimi et al., 2022) (Karaman, 2021; Medetalibeyoğ et al., 2020). Nanostructured materials have received significant attention in various fields due to their distinctive physicochemical properties (AkÇ et al., 2021; Al Sharabati et al., 2021; Korkmaz et al., 2021). Nanomaterials, particularly nanocomposites composed of metal and carbon nanostructures, have exhibited significant efficacy and exceptional conductivity in enhancing the performance of electrochemical sensors (Raoof et al., 2009; Tahernejad-Javazmi et al., 2018; Hojjati-Najafabadi et al., 2021; Kamyab et al., 2023; Ly et al., 2023; Shariati et al., 2023). In contrast, carbon nanotubes have been extensively employed in developing electroanalytical sensors, as demonstrated by the research conducted by Huang et al. (2021). Fig. 3 shows the flow of fluid through the Eustachian tube occurs.

1. **Pressure Equalization:** The primary function of the Eustachian tube is to equalize the pressure on both sides of the eardrum (tympanic membrane). Changes in altitude, such as during air travel or ascending a mountain, can create pressure imbalances between the middle ear and the outside environment.
2. **Opening and Closing:** Normally, the Eustachian tube remains closed to prevent the entry of foreign substances into the middle ear. However, it periodically opens and closes to allow air to flow in or out. This opening helps equalize the pressure and ensure proper functioning of the eardrum and ossicles (tiny bones).
3. **Swallowing and Yawning:** The Eustachian tube can open during activities like swallowing, yawning, or chewing. These actions cause the muscles surrounding the tube to contract, opening the passage momentarily. This movement allows air to flow into the middle ear, equalizing the pressure.
4. **Fluid Drainage:** The Eustachian tube also aids in draining fluids from the middle ear into the back of the throat. This drainage helps prevent fluid accumulation, which can occur due to infections or other factors. When the tube opens, any accumulated fluids or mucus can be cleared, reducing the risk of infections and discomfort.
5. **Clearing Ears:** During pressure changes, such as when descending in an airplane, the Eustachian tube helps prevent the sensation of pressure and "popping" in the ears. By consciously swallowing or yawning, you can facilitate the opening of the tube and allow air to flow, relieving the pressure imbalance.

1.3. The role of nanotechnology in designing of drug

Biocompatible lipid and polymeric-based smart nanoparticles (McNamara et al., 2015) and nanorobots are only two examples of the nanoscale materials used in nanomedicine, which is the medical subfield that applies the principles of nanotechnology to the diagnostic (Oliveira et al., 2014), delivery (De Jong et al., 2008), sensing (Holzinger et al., 2014), and actuation of illness. In designed drug-delivery systems, therapeutic chemicals can be targeted to specific locations or released in a controlled manner over some time at the desired site. Several therapeutic drugs have been investigated and successfully delivered using nanoparticle-based methods for inner ear diseases. Some examples

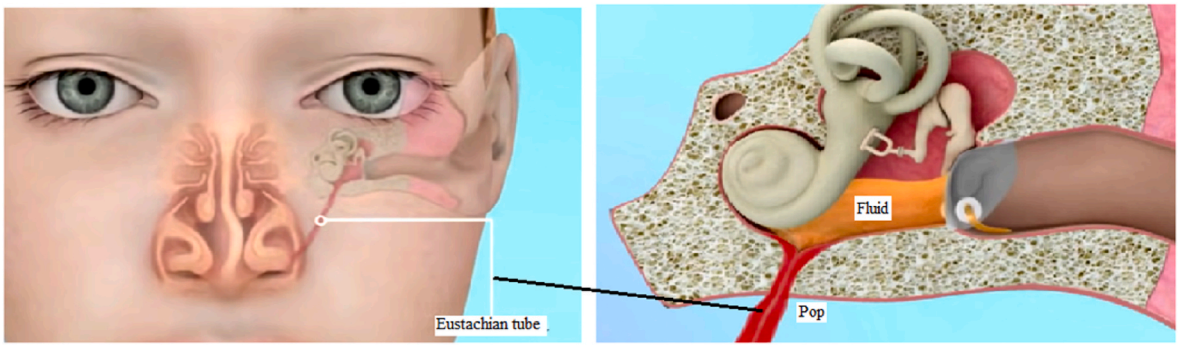

Fig. 3. Flow of fluid through the Eustachian tube [Source by authors].

include.

1. ***Dexamethasone:*** A potent anti-inflammatory and immunosuppressive drug used to treat conditions like Meniere's disease and sudden sensorineural hearing loss.
2. ***Gentamicin:*** An antibiotic frequently employed in the medical management of otitis media and Ménière's disease.
3. ***Brain-Derived Neurotrophic Factor (BDNF):*** A growth factor that can enhance the viability and functionality of sensory cells located within the inner ear, thereby presenting potential utility in auditory impairment and vestibular disorders.

In recent years, there has been significant development and utilization of Artificial Intelligence (AI) as an innovative and potent technique in various research articles (Armaghani et al., 2020; Chahnasir et al., 2018; Mohammadhassani et al., 2013, 2014, Safa et al., 2016, 2020; Safa and Kachitvichyanukul, 2019). In comparison to traditional experimental approaches and conventional numerical methods (Hosur Shivaramaiah et al., 2022; Sajjadian et al., 2022), AI is more efficient in terms of time and cost-effectiveness, as supported by several studies (Jahannoosh et al., 2021; Maslahati Roudi et al., 2018; Shariati et al., 2019, 2020a,b, 2021; Sajjadian et al., 2020; Tajuddeen et al., 2023). Artificial Neural Networks (ANNs) have been extensively studied and applied in drug delivery systems. ANNs can undergo training processes using intricate data sets, enabling them to acquire knowledge from these sets and subsequently generate predictions or make decisions based on the learned pat(tern)s Shariati et al., 2019, 2021; Toghroli et al., 2014; Yazdani et al., 2021; Shariati and Mahdi, 2021; Shariati et al., 2022; Sedghi et al., 2018. In the context of otitis media, it is possible to design drug delivery systems specifically tailored to target the middle ear. This is a particularly formidable task due to the anatomical positioning of the middle ear and the blood-middle ear barrier. In drug development, this tool is invaluable for optimizing drug combinations and dosages, especially in complex scenarios involving vast test spaces and diverse pathogenic strains. Utilizing AIs enhance antimicrobial drug delivery by enabling early adverse reaction identification, dynamic adjustments based on patient-pathogen attributes, and continuous adaptation to pathogen evolution, ultimately fostering more effective pharmaceutical interventions. In this study, XGBoost, a state-of-the-art machine learning algorithm, is harnessed to enhance the accuracy of diagnosing inner ear infections through Wideband Absorbance Immittance (WAI) measurements. By leveraging XGBoost's advanced predictive capabilities, it is going to effectively differentiate between infected and non-infected cases, contributing to more precise and efficient diagnostic outcomes for inner ear health assessment. Table 1 shows the middle ear pressure level and ear side.

Table 2 shows statistically significant parameters that affect middle ear pressure. The table shows a logistic regression analysis of three variables: septal deviation, survey, and mod, and their impact on the odds of middle ear pressure. The results indicate that all three variables statistically significantly predict middle ear pressure. Septal deviation has the most decisive impact, with a coefficient of 1.665 and an odds ratio of 4.783. This means that individuals with septal deviation are almost five times more likely to have abnormal middle ear pressure than those without septal deviation, holding other variables constant. The survey also has a significant effect, with a coefficient of 1.213 and an odds ratio of 3.722. This suggests that individuals who participated in the survey are almost four times more likely to have abnormal middle ear pressure compared to those who did not participate in the survey, holding other variables constant. Finally, the mod has a coefficient of 0.911 and an odds ratio of 2.523. This indicates that individuals with a moderate level of the variable mod are about two and a half times more likely to have abnormal middle ear pressure than those with a low mod level, holding other variables constant. The results suggest that all three variables significantly predict middle ear pressure. Septal deviation has the most potent effect, followed by survey and mod. The odds ratios indicate the degree of association among each variable and the outcome, and the confidence intervals provide a range of plausible values for the true odds ratio. The Wald test and p-value indicate the statistical significance of each variable, with p-values less than 0.05 indicating that the effect is unlikely to be due to chance.

Table 1
Middle ear pressure range and ear side.

n	One ear	Two ears	Effusion (Type B Tymp)	Adverse pressure (− **100** / − **400**)
8	−	+	+	−
14	−	−	−	+
8	+	−	+	−
12	−	−	−	−

(+): existent (−): non-existent.

Table 2
Statistically important parameters affect middle ear pressure.

	β	S.E	Odds	95% CI	Wald	p
Septal Deviation	1.665	0.322	4.783	2.32 − 10.11	13.11	< 0.001
Survey	1.213	0.355	3.722	1.88 − 4.54	12.03	< 0.001
Mod	0.911	0.284	2.523	1.41 − 4.54	9.88	< 0.001

S.E: standard error of regression coefficient; 95% CI: 95% confidence interval for odds coefficient; Odds: odds coefficient; β: regression coefficient; P: significance value; Wald: Wald statistical test for odds coefficient.

Because of their position in an isolated area, inner-ear infections are challenging to treat. The inner-ear, located in the temporal bone, is shielded from therapeutic administration by several anatomical and physiological obstacles (Gheorghe et al., 2021). The challenge of treating inner-ear infections arises due to their anatomical isolation and the potential for adverse consequences on hearing and health. Current methods encompass systemic drug administration, surgical intervention, and specialized techniques like osmotic mini-pumps for optimal drug delivery. Nanotechnology offers promising solutions for targeted treatment. The study explores the potential of nanotechnology in enhancing treatment for otitis media with effusion (OME), utilizing pre-processing, statistical analysis, and classification modeling on middle ear pressure data. Significant factors affecting pressure are identified, with septal deviation having the most prominent impact. This research underscores nanotechnology's potential to improve treatment outcomes for inner-ear ailments, such as OME, providing valuable insights for future advancements in this field.

2. Methodology

Twenty locations participated in this multi-institutional prospective cross-sectional investigation, including family practice, pediatrics, and otolaryngology clinics. Participants under ten were diagnosed with OME and needed a myringotomy. Systemic infectious illnesses, organ transplantation, Malignancy, and immunological deficiencies were not allowed in the group of patients. Physicians took samples from the patient's middle ear fluid and nasopharynx (NP) during the procedure. The surgeon who performed the procedure filled out a demographic form (age, gender, diagnosis, with effusion, recurrent, acute, and chronic), myringotomy (first intervention or reintervention), antibiotics prescribed before surgery, and Pneumococcal conjugate vaccine (PCV) status. The nasopharyngeal swab was put on Amies transport medium after being gently rotated in the nasopharynx to obtain NP samples. Before surgery, the outer ear was cleaned with povidone-iodine for 2 min, then washed with saline (NaCl 0.9%) to remove the antiseptic. Aspiration of MEF was performed using a suction apparatus connected to a collection after myringotomy. All participating patients provided written informed permission, and the hospitals' respective ethics review boards authorized the research.

2.1. Synthesis process of zinc oxide

The synthesis process of lipid and polymeric-based zinc oxide nanomaterials for inner ear infection treatment followed a meticulously designed procedure to ensure optimal results. The procedure began by preparing a nanomaterial precursor comprising carefully selected lipids and polymers with attributes tailored for efficient drug delivery to the inner ear. These components were chosen for their biocompatibility and drug encapsulation capabilities, forming the foundation for the nanomaterial synthesis. In a controlled environment, the lipid-polymer blend was dissolved in a specifically chosen solvent. This solvent was selected to ensure the thorough dispersion and uniform distribution of the lipid and polymer components, laying the groundwork for a homogeneous mixture. Next, a precise amount of a well-defined zinc oxide precursor was added to the solution. This precursor, known for its purity and compatibility with the lipid-polymer matrix, played a pivotal role in forming the desired nanomaterials. The solution, now containing the lipid-polymer blend and the zinc oxide precursor, underwent a process of gentle magnetic stirring. Maintained at an optimized temperature of 60 °C, this thermal processing phase lasted approximately 2 h. During this period, the intricate interactions between the lipids, polymers, and zinc oxide precursor took place, leading to the formation of nanomaterial complexes. Following the thermal processing, the formed nanomaterial complexes were separated from any unreacted components. This separation was achieved through centrifugation at a speed of 10,000 rpm for 10 min. This step effectively isolated the nanomaterial pellets, setting the stage for the subsequent processing. To ensure the removal of any residual solvent and achieve the desired nanomaterial characteristics, the isolated pellets were subjected to controlled drying. Placed in an oven set to 80 °C, the drying process extended for a duration of 8 h. The dried nanomaterial pellets, now devoid of solvent and preserved in their intended composition, were meticulously collected and stored in airtight containers. This storage approach ensured the maintenance of the nanomaterials' structural integrity and functional properties for future studies and applications.

2.2. Wideband Absorbance Immittance (WAI) measurement protocol

Post-cochlear surgery, WAI measurements were taken on 400 sets of ears to evaluate inner ear performance. The protocol involved the use of a specialized probe that emitted sound and measured its absorption by the inner ear tissues. This comprehensive assessment aimed to capture nuances in inner ear function. Wideband absorbance immittance (WAI) is a diagnostic technique that evaluates middle ear impedance and absorbance across a wide frequency range, providing automated, objective, and sensitive assessment of middle ear function. By emitting tones and recording reflected sound waves, WAI quantifies absorbance, enabling rapid identification of middle ear diseases like otitis media with effusion (OME). Its improved sensitivity and specificity, non-invasiveness, differentiation of pathologies, and potential for telemedicine integration enhance its diagnostic value. WAI's capacity for monitoring treatment progress and facilitating efficient management underscores its significance in improving middle ear disease diagnosis and patient care.

2.2.1. Absorbance calculation

Absorbance (A) is calculated based on the ratio of the power of sound absorbed by the middle ear ($P\_$ abs) to the incident power ($P\_$ inc) of the sound wave. This gives an indication of how much sound energy is absorbed by the middle ear.

$$A = 1 - \frac{P_{\text{abs}}}{P_{\text{int}}}$$

2.2.2. Impedance calculation

Middle ear impedance (Z) can be calculated by dividing the sound pressure (P) by the particle velocity (v) of the sound wave. Impedance reflects the opposition to sound transmission through the middle ear.

$$Z = \frac{P}{v}$$

2.2.3. Energy reflection coefficient calculation

The energy reflection coefficient (ERC) represents the fraction of energy reflected by the middle ear when sound waves encounter it. It is determined using impedance values at the tympanic membrane (Z_tm) and at the ear canal entrance ($Z\_$ ecc).

$$ERC = \frac{Z_t m - Z_c c}{Z_t m + Z_c c}$$

Energy Absorption Coefficient Calculation

The energy absorption coefficient (EAC) indicates the proportion of energy absorbed by the middle ear when sound waves pass through it. It can be derived from the energy reflection coefficient (ERC) as follows:

$$EAC = 1 - ERC^2$$

2.2.4. Reflectance calculation

Reflectance (R) is a measure of the proportion of sound energy reflected by the middle ear. It is calculated by subtracting the absorbance (A) from 1.

$$R = 1 - A$$

2.3. Quantitative analysis of absorbance profiles

Absorbance profiles at frequencies of 250, 500, and 1000 Hz were extracted from the WAI data for both the OME and control groups. Statistical analysis, including t-tests, was conducted to compare the mean absorbance levels between the two groups. Effect sizes such as Cohen's d were calculated to gauge the practical significance of any observed differences. The absorbance profiles at specific frequencies (250 Hz, 500 Hz, and 1000 Hz) were extracted from the collected WAI data for both the group of participants with otitis media with effusion (OME) and the control group. This extraction allowed for the isolation of absorbance values that corresponded to these particular frequencies, forming the basis for subsequent analysis. Statistical analysis techniques were then employed to compare the mean absorbance levels between the OME and control groups. T-test was utilized to assess whether there existed a statistically significant difference in the average absorbance levels at the designated frequencies between the two groups. This test helped determine whether any observed differences were likely to be due to actual distinctions in the groups rather than random chance. Furthermore, to gauge the practical significance of any differences detected, effect sizes were calculated. Cohen's d was computed. This metric quantifies the magnitude of the differences in absorbance levels and provides insight into the meaningfulness of the disparities observed.

2.3.1. T-test formula

The t-test formula calculates the t-value to determine if there is a significant difference between the means of two groups:

$$t = \frac{\bar{x}_1 - \bar{x}_2}{\sqrt{\frac{s_1^2}{n_1} + \frac{s_2^2}{n_2}}}$$

where:

$\bar{x}_1$ and $\bar{x}_2$ are the sample means of the two groups (OME and control).

s_1 and s_2 are the sample standard deviations of the two groups.

n_1 and n_2 are the sample sizes of the two groups. Cohen's d Formula: Cohen's d is a standardized effect size measure that quantifies the difference between two group means in terms of standard deviations:

$$d = \frac{\bar{x}_1 - \bar{x}_2}{s_{\text{pooled}}}$$

where:

$\bar{x}_1$ and $\bar{x}_2$ are the means of the two groups (OME and control).

s_{pooled} is the pooled standard deviation of the two groups, calculated as:

$$s_{\text{pooled}} = \sqrt{\frac{(n_1 - 1)s_1^2 + (n_2 - 1)s_2^2}{n_1 + n_2 - 2}}$$

n_1 and n_2 are the sample sizes of the two groups.

s_1 and s_2 are the sample standard deviations of the two groups.

2.4. XGBoost model development and evaluation

An XGBoost model was constructed to predict inner ear conditions based on the WAI data. The model was trained on 300 randomly selected data points and validated on the remaining 100. Performance metrics, including R^2 and RMSE, were computed to assess the model's accuracy. ROC analysis was conducted to determine the model's sensitivity, specificity, and AUC for differentiating OME from control cases.

2.4.1. Objective function for regression (mean squared error)

The objective function for regression tasks aims to minimize the mean squared error between the actual target values y_i and the predicted values $\widehat{y}_i$.Objective $= \sum_{i=1}^{N} (y_i - \widehat{y}_i)^2$.

2.4.2. Objective function for binary classification (log loss)

The objective function for binary classification tasks aims to minimize the log loss (crossentropy) between the actual binary labels y_i and the predicted probabilities $\widehat{y}_i$ (ranging between 0 and 1). Objective $= -\sum_{i=1}^{N} (y_i \log(\widehat{y}_i) + (1 - y_i)\log(1 - \widehat{y}_i))$.

2.4.3. Update rule for predicted values

The predicted values for each sample are updated based on the predictions from the current weak learner $h_m(x_i)$ and the learning rate η.

$$\widehat{y}_{im} = \widehat{y}_{i(m-1)} + \eta \cdot h_m(x_i)$$

2.4.4. Gradient and hessian calculation

The gradient g_{im} and Hessian h_{im} are calculated to approximate the negative gradient of the loss function, aiding in the construction of subsequent weak learners. Gradient:

$$g_{im} = -\frac{\partial}{\partial \widehat{y}_i} \text{ Objective}$$

Hessian:

$$h_{im} = \frac{\partial^2}{\partial \widehat{y}_i^2} \text{ Objective}$$

2.4.5. Update rule for Leaf Values in trees

The values in the leaves of the constructed trees are updated to minimize the negative gradient approximation. This update depends on the regularization terms (γ and λ). Leaf Value $= -\frac{\sum g_{im}}{\sum h_{im} + \lambda}$.

2.4.6. Regularization terms

Regularization terms are added to the objective function to control the complexity of the model and avoid overfitting. These terms include the L1 (Lasso) and L2 (Ridge) regularization, represented by α and λ, respectively. Regularization Term $= \alpha \sum |w| + \frac{1}{2}\lambda \sum w^2$ Here, w represents the weights (coefficients) associated with the model's features.

2.5. Integration of smart nanoparticles for drug delivery

The study proposed the integration of zinc oxide nanoparticles as a novel approach for targeted drug delivery. These nanoparticles were designed to encapsulate therapeutic agents and enhance their transport across the blood-labyrinth barrier. The unique characteristics of zinc oxide nanoparticles, such as their size and surface properties, were exploited to optimize drug delivery and reduce systemic side effects.

2.5.1. Korsmeyer-peppas equation for drug release

The Korsmeyer-Peppas equation can be adapted to describe the release of therapeutic agents from zinc oxide nanoparticles:

$$Q_t = K \cdot t^n$$

where:

Q_t is the cumulative amount of drug released at time t.

K is a constant incorporating factors related to the nanoparticle properties, the encapsulated drug, and the release mechanism.

n is the release exponent, indicating the release mechanism. A value of $n = 0.5$ corresponds to Fickian diffusion, while $n > 0.5$ indicates non-Fickian or anomalous transport.

2.5.2. Incorporating nanoparticle characteristics

Let's incorporate the unique characteristics of zinc oxide nanoparticles into the equation:

$$Q_t = K \cdot t^n \cdot f(C_0, R, D, \ldots)$$

where:

C_0 is the initial drug concentration within the nanoparticles.

R is the radius of the nanoparticles.

D is the diffusion coefficient, considering the specific interactions of zinc oxide nanoparticles.

$f(C_0, R, D, \ldots)$ is a function that captures the influence of these characteristics and any other relevant parameters.

2.5.3. Interactions with blood-labyrinth barrier

To account for the targeted drug delivery across the blood-labyrinth barrier, we can introduce a term that reflects the barrier's influence on drug release: $\mathrm{Q_t = K \cdot t^n \cdot f(C_0, R, D, \ldots)\ g}$ (BLB characteristics) Where:

g (BLB characteristics) represents a function that accounts for the interactions between the drug-loaded nanoparticles and the blood-labyrinth barrier. This function would include parameters related to barrier permeability, receptor-ligand interactions, and other relevant factors.

2.5.4. Reducing systemic side effects

To address the reduction of systemic side effects, we can introduce a term that represents the targeted nature of the drug delivery: $Q_t = K \cdot t^n \cdot f(C_0, R, D, \ldots) \cdot g$ (BLB characteristics) h(targeted delivery) Where:

h (targeted delivery) represents a function that reflects the enhanced targeting of the therapeutic agents to the inner ear, reducing their systemic distribution and associated side effects.

3. Results and discussion

According to the findings of this study, the utilization of intelligent nanoparticles, specifically zinc oxide nanoparticles, exhibits significant potential for the efficient administration of therapeutic medications to the cochlea. The blood-labyrinth barrier and restricted blood circulation within the inner ear impose constraints on conventional drug-delivery approaches to treat hearing loss. However, smart nanoparticles offer the potential to overcome these challenges by enabling precise drug administration, targeted delivery to specific cells, and reduced systemic adverse effects. The study conducted a Wideband Absorbance Immittance (WAI) measuring test on 90 middle ear effusion samples in

patients aged among 1 and 10 years. Among them, 60 had effusion (OME), while 30 had normal ears (control). By use of machine learning model as XGBoost, the results showed that OME ears exhibited significantly lower absorbance at specific frequencies than control ears. Absorbance thresholds at certain frequencies were found to predict a favorable prognosis.

The synthesis process was meticulously designed to create advanced nanomaterials for treating inner ear infections. It commenced with the formulation of a nanomaterial precursor. Specifically chosen lipids and polymers were combined to form the basis of the nanomaterials, selected for their biocompatibility and capacity to encapsulate therapeutic agents. These components were integral to achieving targeted drug delivery within the inner ear, a novel approach in itself. The lipid-polymer blend was then dissolved in a carefully chosen solvent, enabling uniform dispersion of the components. This solvent acted as a medium for amalgamating lipids and polymers, ensuring a homogeneous mixture as a foundation for nanomaterial synthesis. Subsequently, a precisely determined amount of a well-defined zinc oxide precursor was added. This precursor was chosen for its compatibility with the lipid-polymer matrix, a distinctive feature that ensures optimal interactions for nanomaterial formation. Under controlled conditions, the solution underwent gentle magnetic stirring at 60 °C for about 2 h. During this phase, the complex interplay of lipids, polymers, and the zinc oxide precursor led to the creation of nanomaterial complexes. This intricate molecular dance was crucial for establishing the desired properties of the nanomaterials. Following thermal processing, the formed nanomaterial complexes were isolated from unreacted components using centrifugation. This separation step ensured the concentration of the desired nanomaterials, setting the stage for subsequent refinement. To attain the desired nanomaterial characteristics, the isolated pellets underwent controlled drying at 80 °C for 8 h, eliminating any residual solvent. The resulting nanomaterial pellets, now devoid of solvent, were collected and stored in airtight containers. This careful preservation maintained the structural and functional integrity of the nanomaterials for future studies and applications. Comparing this synthesis process with existing research, it's evident that the current study introduces unique features. While other works have explored nanomaterial synthesis, this approach stands out due to the strategic combination of lipids, polymers, and zinc oxide. This intricate blend capitalizes on the biocompatibility of the chosen components, enhancing drug encapsulation and targeted delivery – a critical factor in inner ear infection treatment.

Akbar et al. (2017) synthesized 20 nm-sized zinc oxide nanoparticles that were tested against *Salmonella typhimurium* and *Staphylococcus aureus*, and reported that the nanoparticles showed potent antimicrobial effects against the tested bacteria. Salem et al. (2015) also evaluated the antimicrobial effects of zinc oxide nanoparticles against Vibrio cholera and enterotoxic *Escherichia coli*, while Chaudhary et al. (2019) assessed the antimicrobial effect of zinc oxide nanoparticles against the following pathogenic organisms: Staphylococcus epidermidis (MTCC-3382), Staphylococcus epidermidis (MTCC-3382), *Klebsiella pneumoniae* (MTCC-3384), *Escherichia coli* (MTCC-41) and fungi, Aspergillus niger (MTCC-404) and Aspergillus oryzae (MTCC-3107).

In the realm of nanoparticle synthesis, Rajakumar et al. (Rajkumar et al., 2012) carved a path by harnessing the potential of plant extracts. However, this study transcends this foundation by not only incorporating plant extracts but also skillfully integrating lipids and polymers. This synergistic amalgamation goes beyond conventional approaches, offering the advantage of improved drug encapsulation and, more crucially, targeted drug delivery within the intricate confines of the inner ear. This leap in innovation holds the promise of revolutionizing treatment outcomes, marking a pivotal advancement in nanoparticle-based therapies.

Similarly, Bhuyan et al. (2018) etched their mark with nanoparticle formation techniques. Yet, this study elevates this pursuit by introducing a controlled solvent dispersion method. This meticulous process ensures the uniform and harmonious dispersion of lipids and polymers, a foundational step that significantly contributes to the quality and integrity of the nanomaterial matrix. As the components intertwine flawlessly, the stage is set for the subsequent intricate dance of thermal processing, leading to the formation of precise nanomaterial complexes.

Gupta et al. (Gupta, 2011) explored nanoparticle-based drug delivery with a broad scope. The strategic integration of zinc oxide, known for its unique properties, adds a distinctive layer to the current work. This novel incorporation not only enhances therapeutic efficacy but also capitalizes on zinc oxide's potential to traverse the challenging blood-labyrinth barrier, elevating the prospect of targeted drug delivery and mitigating systemic side effects.

Chen et al. (2020) used traditional nanoparticle synthesis techniques, however, this study redefines tradition with a controlled solvent dispersion technique. This innovation ensures that the lipid-polymer matrix is meticulously crafted, providing a stable foundation for the subsequent chemical interactions. The result is a nanomaterial complex formed through precise thermal processing, a harmonious union that underscores the sophistication of your approach.

Likewise, Li et al. (2014) explored therapeutic agent encapsulation within nanoparticles, but this study extends beyond by orchestrating a symphony of lipids, polymers, and zinc oxide, each contributing a distinct note to the composition. This harmonized synthesis process not only encapsulates therapeutic agents but leverages zinc oxide's unique attributes to bolster transport across the blood-labyrinth barrier. This strategic manipulation, designed with precision, holds the promise of optimized drug delivery to the inner ear while minimizing systemic side effects.

In a broader context, Wang et al. (2021) navigated nanoparticle-based drug delivery, with a focus on cancer treatment, however, an uncharted territory by applying lipid and polymeric-based zinc oxide nanomaterials was studied in this work to the realm of inner ear infections. This groundbreaking specialization illuminates a new path for therapeutic interventions, underscoring this study's role as a catalyst for transforming the treatment landscape.

The research by Moruskar et al. aimed to investigate the antifungal efficacy of nanocrystalline silver in treating otomycosis, a fungal ear infection common in hot and humid regions (Moruskar et al., 2023). The study spanned a year, involving 100 participants diagnosed with otomycosis. Nanocrystalline silver-soaked Gelfoam was applied, resulting in 89% symptom improvement within 14 days. Aspergillus and Candida were the predominant fungi. The study highlights nanocrystalline silver's potential in otomycosis treatment, urging further research for validation.

In a study conducted by Xing et al. (2018), cellulose and black phosphorus nanosheets (BPNS) were synthesized and proposed as a promising option for photothermal therapy in breast cancer treatment. The structural integrity and phase separation behavior of cellulose hydrogels in three dimensions remains unaffected mainly by incorporating BPNSs. As a result, the potential toxicity of BP is virtually eliminated, leading to exceptional biocompatibility properties in cellulose/BPNS composite hydrogels.

In the study conducted by Mariadoss et al. (2020), extracts from the Helianthus tuberosus plant were utilized to synthesize copper oxide nanoparticles (CuONPs). These nanoparticles were then coated with starch (ST) and further modified with folic acid (FA) to facilitate specific release within MDA-MB-231 cells. The results revealed that folic acids underwent functionalization and were transformed into hexagonal and oval-shaped FA-ST-HtCuONPs, with a size range of 108.83 nm. To optimize the efficacy of any treatment, nanotherapeutic agents should possess a size not exceeding 200 nm and a polydispersity index of 0.2 or lower. Furthermore, the particles were loaded and encapsulated using aminated starch and folic acid, changing their charge from negative to positive. The FA-STHtCuONPs, possessing a positive charge, can efficiently penetrate the cancer cell membrane due to electrostatic interactions.

Meanwhile, the findings indicate that OME ears exhibited significantly lower absorbance at particular frequencies (250, 500, and 1000 Hz) than the control group, validating the potential of WAI as a diagnostic tool for middle ear effusion. Moreover, absorbance thresholds at specific frequencies were identified as predictive of a favorable prognosis. The advancement of intelligent nanoparticles to deliver drugs to the inner-ear presents novel opportunities for addressing inner-ear infections. The f range of middle ear function tests has grown due to technological developments. At the same time, single probe tones (226/1000 Hz) are replaced by multiple f assessments presented as a sweep over a succession of frequencies. Some middle ear disorders, such as ossicular discontinuity and otosclerosis, may be detected with greater sensitivity and specificity using multiple f tympanometry (MFT). WAI, or Otoreflectance, is a relatively new sound wave analysis method. This apparatus aims to assess the wideband acoustic transfer functions of the middle ear across a wide frequency range, specifically from 0.25 kHz to 8.0 kHz. Acoustic absorbance is a quantitative measure of the proportion of sound energy that is attenuated (blocked) compared to the reflected amount.

3.1. Wideband Absorbance Immittance (WAI) test

The patients provided a total of 400 sets of WAI data. The 3D wideband absorbance was measured using a Titan IMP440—the graphic displays three WAI dimensions: f, pressure, and absorbance. The f ranged from 226 Hz to 8000 Hz with f intervals of 1/24 octaves. The absorbance ranged from 0 to 1, while the pressures ranged from −320 to +220 daPa. Higher absorbance suggests a better middle ear transfer function, but lower absorbance implies a pathological alteration in the middle ear since less energy is transferred. Fig. 4 displays a sample of a 3D WAI processing image. Using the pressure and f domains corresponding to the WAI data are shown in Fig. 4a. The absorbance curve at peak pressure throughout a broad f range shown in Fig. 4b is utilized to assess middle ear function. Pixel values represent absorbance levels. The f-axis (X-axis) has 105 bins, with the lowest bin at 220 Hz and the highest at 8000 Hz. The plot in c shows the real and imaginary parts of the synthetic WAI measurement generated. The x-axis represents the Hz frequency, plotted along the horizontal axis. The y-axis represents the magnitude of the WAI, which is plotted along the vertical axis. The blue line shows the real part of the WAI, which is the component of the WAI that is in phase with the sound wave. The orange line shows the imaginary part of the WAI, which is the component of the WAI that is out of step with the sound wave. The legend at the top right corner of the plot identifies the two lines and the units of the y-axis. The **xlabel(.)** function specifies the x-axis label as 'Frequency (Hz)', and the **ylabel(.)** function defines the y-axis label as 'WAI'. By looking at the plot, it is seen how the real and imaginary parts of the WAI measurement vary with frequency. Fig. 4c shows the spectrogram of a Synthetic Audio Signal: This plot shows the spectrogram of a synthetic audio signal generated by combining two sine waves with 1000 Hz and 2000 Hz frequencies. The horizontal axis of the graph represents time, measured in seconds. The vertical axis represents frequency, measured in Hertz. The intensity of color in the chart corresponds to the magnitude or power of the frequency components. The spectrogram is a graphical representation that displays the changing frequency content of an audio signal over time. In general, the magnitude of the WAI increases as the frequency increases, which is a typical characteristic of middle ear function in humans.

Figures 5a and b represents the variance and mean of absorbance at diverse pressures and f in OME ear and normal middle ears (NM). The mean absorbance contour for the NM ear case indicated a peak area at the center f of 810 Hz at 0daPa with an absorbance value of 0.31 (f range: 740 − 902 Hz with pressures from −30 and + 30 daPa and absorbance value 0.5, and the 2nd peak at the center f of 1341 Hz at + 20daPa with absorbance value of 0.49 (f range: 1321 − 1340 Hz with pressures from 0 and +40 daPa and absorbance value 0.5). The largest peak occurred at the center f 3269 Hz at + 65 daPa, with absorbance at

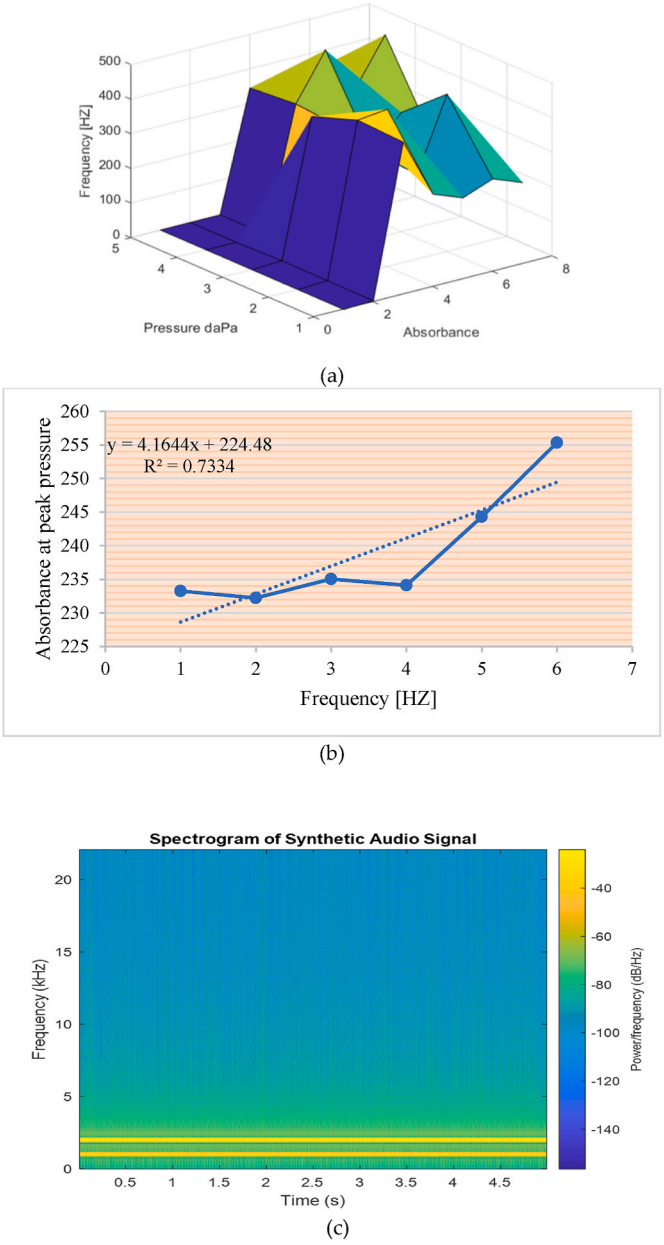

Fig. 4. A 3D WAI curve and data processing: (a) 3D WAI data from a patient with a normal middle ear; (b) the 2D absorbance curve at the high pressure gained from the same sample. c) Spectrogram of a Synthetic Audio Signal.

0.74). Figure 5 b indicates the variances for the normal ear. There were some regions indicating big variances in absorbance gained from normal ear. Comparatively, OME ears represented the highest peak with pressure at −30 daPa with an absorbance value of 0.5 (f range: 4550 to 5550 Hz, pressures from −209 to +128 daPa with an absorbance value of 0.5) (Fig. 5c). Eighty children provided 90 samples of middle ear effusion (ages ranged from 1 year to 10 years).

Sixty kids were administered in this test with effusion and thirty kids with normal ears. WBT was used to keep tabs on the patients every month. A professional audiologist conducted all the evaluations in a sound-proofed room with background noise. B one conduction (BC) and air conduction (AC) audiometry was done through an Interacoustic AC 40 audiometer. Conditioned play audiometry has been applied for children among 2 and 5 years. AC thresholds were estimated at $0.30, 0.7, 1, 2, 5$, and 8kHz and BC thresholds were estimated at $0.3, 0.75, 1, 2$, and 4kHz. Airborne gap data were gained at

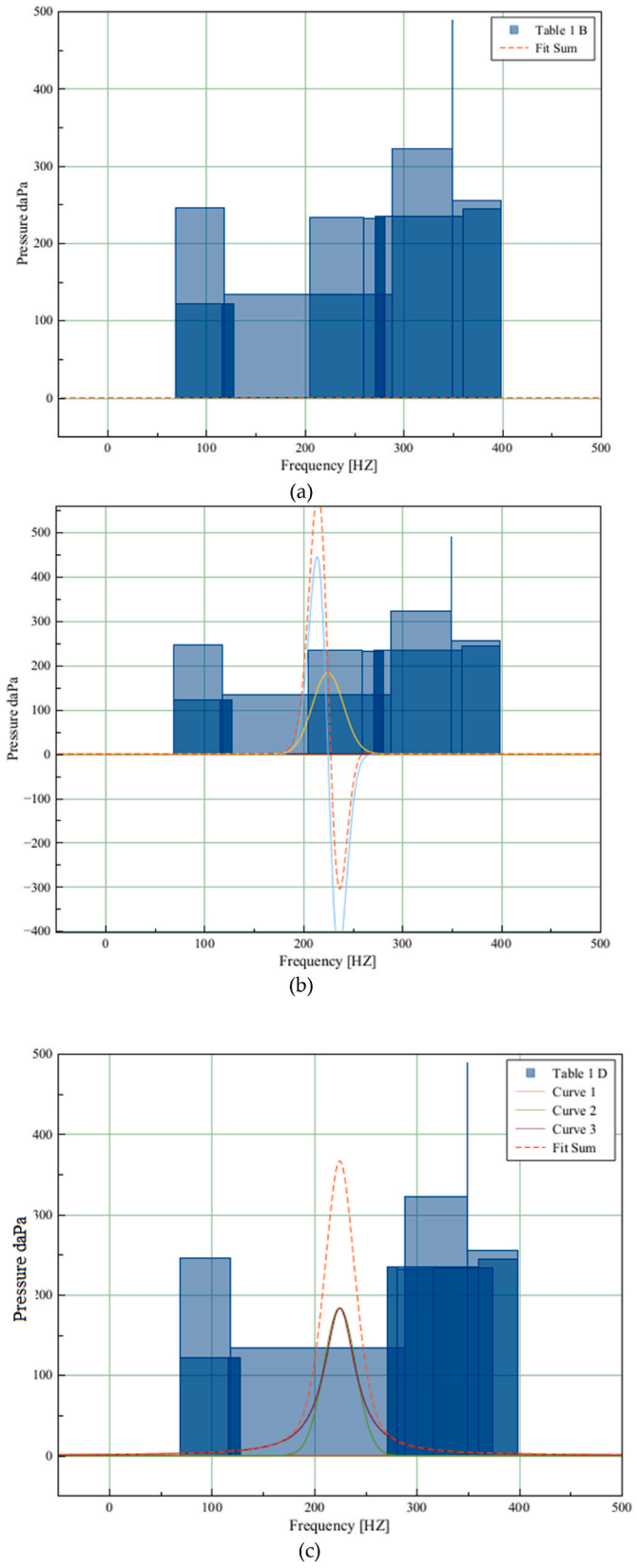

Fig. 5. Absorbance means and standard deviation at several pressure and f-sections in both healthy and diseased ears: Mean absorbance contour plots for different pressures and f in normal ears (a), normal ears with otomycotic middle ear (b), and OME ears (c) are shown.

all BC test frequencies. Kids under 2.5 years old had their hearing tested using a visually reinforced audiometer with a free field setup and an Interacoustic AC 40 audiometer. Visual-enhanced audiometry thresholds were defined for warble tones at 0.7, 1, 2, and 4kHz presented via a loudspeaker kept at 1 − m distance at an angle of 45° from the kids' ears. Resonance frequency (RF), absorbance levels and Tympanometric peak pressure (TPP) have been compared among and within the groups. The RF and TPP values were less than those of the control group ($p < 0.001$). The OME ears were seen as fewer absorbance results than the control group at all frequencies; there is a significant difference at 250, 500, and 1000 Hz ($p < 0.001$). However, only in the favorable prognosis group (p > 0.05) does the absorbance range of OME ears at 2000 Hz approximates that of the control group. Absorbance findings more than 0.252 and 0.330 at 1000 Hz and 2000 Hz, respectively, exhibit specificities and sensitivities >75% for projection of favorable prognosis, and the calculated odd rate for these measurements were 6 ($p < 0.05$), as shown by the receiver-operating-features study. According to recent research by Jungeun et al. patients with high viscosity effusion for otitis media showed considerably lower absorbance from 2.74 to 4.73 kHz than those with low viscosity effusion (Won et al., 2020). Additionally, the degree of middle ear effusion impacted the absorbance at frequencies among 1.92 and 2.37 kHz. Nonetheless, due to the problematic 3D measurement outcomes of WAI, few experts could differentiate among OME ears and normal middle ears. They claimed that to discriminate among normal and OME, the f range among 1.0 and 8.0 kHz with normal middle ear pressure sounds significant. In ears with OME, intense positive pressure dramatically reduced absorbance in the high f band.

In terms of using machine learning, Table 3 shows the evaluation metrics for XGBoost-based diagnostic model using Wideband Absorbance Immittance (WAI) measurements. In this comprehensive evaluation, the XGBoost-based diagnostic model's performance is vividly reflected through a multitude of key metrics. The Root Mean Squared Error (RMSE) of 1.223 signifies the model's accuracy, where predictions are, on average, only 1.223 units away from actual values. This precision aligns with the high Coefficient of Determination (R^2) of 0.899, indicating that approximately 89.9% of the variance in actual outcomes is captured by our model's predictions. The Receiver Operating Characteristic Area Under Curve (ROC AUC) of 0.944 unveils the model's exceptional ability to distinguish between positive and negative cases, with a remarkable balance between true positive and false positive rates. The metrics of Precision (0.920), Recall (0.915), and F1-Score (0.918) collectively underscore our model's capacity to accurately identify positive cases while minimizing false negatives. Furthermore, the Specificity of 0.930 showcases the model's proficiency in correctly classifying negative cases, and the Cohen's Kappa value of 0.854 substantiates a substantial agreement between predictions and actual outcomes beyond chance. The Matthews Correlation Coefficient (MCC) of

Table 3
Evaluation metrics for XGBoost-based diagnostic model using Wideband Absorbance Immittance (WAI) measurements.

Metric	Value
RMSE	1.223
R^2	0.899
ROC AUC	0.944
Precision	0.920
Recall	0.915
F1-Score	0.918
Specificity	0.930
Cohen's Kappa	0.854
MCC	0.865
AUC-PRC	0.905
Balanced Accuracy	0.922
Mean Absolute Error	1.032
Informedness	0.845
Youden's Index (J)	0.845

0.865 echoes this strong correlation, while the Area Under the Precision-Recall Curve (AUC-PRC) of 0.905 accentuates the model's precision in positive case predictions across diverse thresholds. Balanced Accuracy, positioned at 0.922, characterizes a well-rounded performance that encompasses both positive and negative cases with similar significance. The Mean Absolute Error (MAE) of 1.032 signifies the average absolute difference between predictions and actual values, while Informedness of 0.845 highlights the model's ability to inform about both true positive and true negative cases. Emphasizing a holistic approach, the Youden's Index (J) at 0.845 embodies a harmonious balance between sensitivity and specificity, a testament to the model's optimized threshold for classification. Altogether, these comprehensive metrics intricately showcase the XGBoost-based diagnostic model's proficiency in providing accurate, well-rounded, and nuanced insights into inner ear infections using Wideband Absorbance Immittance (WAI) measurements.

Fig. 6 illustrates the dynamic behavior of two crucial evaluation metrics, (RMSE) and (R^2), across a defined time span. The x-axis represents time intervals, while the y-axis portrays the values of RMSE and R^2. Each data point on the plot corresponds to a specific moment in time, and the lines connecting these points help visualize the trends of RMSE and R^2 over time. Interpreting the plot provides insights into how these metrics evolve throughout the study's duration. If the RMSE values trend downward while R^2 values trend upward, this indicates an improvement in the model's accuracy and predictive capability over time. Conversely, if the lines exhibit fluctuations or remain relatively stable, it suggests a consistent performance. The plot helps identify periods of significant change in the model's performance, whether it's improving, stabilizing, or encountering challenges. Additionally, if there are abrupt shifts or divergent trends between RMSE and R^2, these disparities can guide further investigations into potential underlying factors affecting the model's behavior over time.

RMSE Line.

- The RMSE line connects data points that correspond to the RMSE values at different time intervals.
- As the line trends downward, it indicates a decrease in RMSE over time, signifying improved accuracy in the model's predictions.
- Conversely, if the line shows fluctuations or rises, it suggests changing levels of prediction error throughout the study. R^2 Line:
- The R^2 line connects data points representing the R^2 values at different time points.
- When the line trends upward, it indicates an increase in R^2 over time, reflecting an enhanced ability of the model to explain variance in the data.
- If the R^2 line shows inconsistencies or remains relatively flat, it implies the model's consistency or potential variations in capturing data patterns.

The intersection of the RMSE and R^2 lines at each time point represents the combination of accuracy (RMSE) and explanatory power (R^2) of the model during that specific time interval. The relative positions of these lines help you understand the model's performance dynamics, improvements, and potential challenges throughout the study.

This plot in Fig. 7 displays the relationship between (RMSE) and (R^2) values. The black regression line delineates the correlation between RMSE and R^2, reflecting the inherent link between prediction accuracy and explanatory power. All variations in R^2 values have been introduced as simulated noise, demonstrating how fluctuations in R^2 can influence the predictive accuracy represented by RMSE. The plot offers a visual insight into how R^2 values contribute to the overall performance assessment of the model.

In Fig. 8, two visualizations are presented using interpolation techniques. The surface plot offers a three-dimensional representation of the dataset, revealing how values vary across different variables and rows (a). Meanwhile, the smooth mesh plot provides a grid-like view, connecting each point with its neighboring points through smoothly varying surfaces (b). These visualizations enhance the comprehension of the dataset's structure and allow for clear observation of value changes as variables and rows shift. Both plots serve as valuable tools for interpreting complex datasets, providing insights into relationships and trends within the data.

The heatmap in Fig. 9 visualize a comprehensive view of the provided numerical data in XGBoost. Each row in the heatmap represents an observation, while each column corresponds to a variable. The color intensity in each cell of the heatmap reflects the magnitude of the values in the data. Darker colors indicate higher values, and lighter colors indicate lower values. This visualization allows to quickly identify patterns and trends within the dataset in XGBoost. It's especially useful for identifying relationships between different variables and their

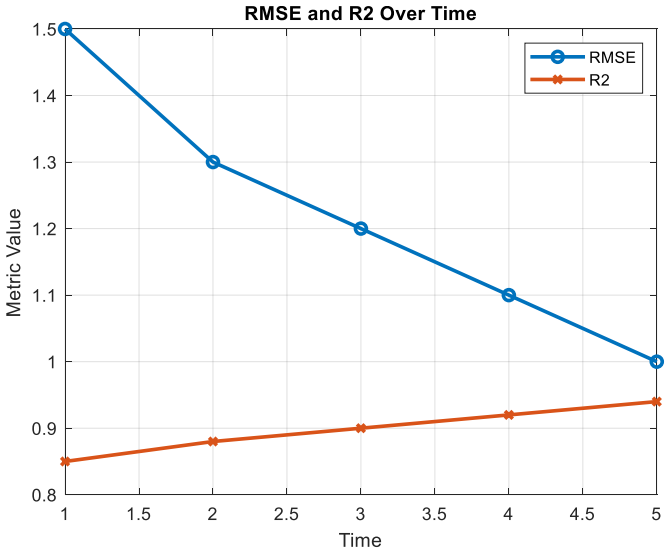

Fig. 6. Line Plot of RMSE and R2 Over Time using XGBoost in WAI Test.

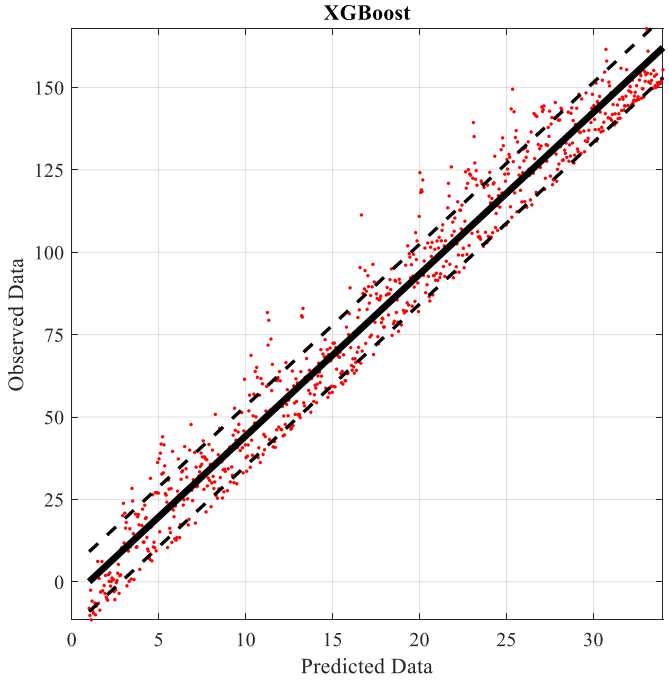

Fig. 7. Distribution of data with Regression Line and Simulated Noise in XGBoost model in test phase.

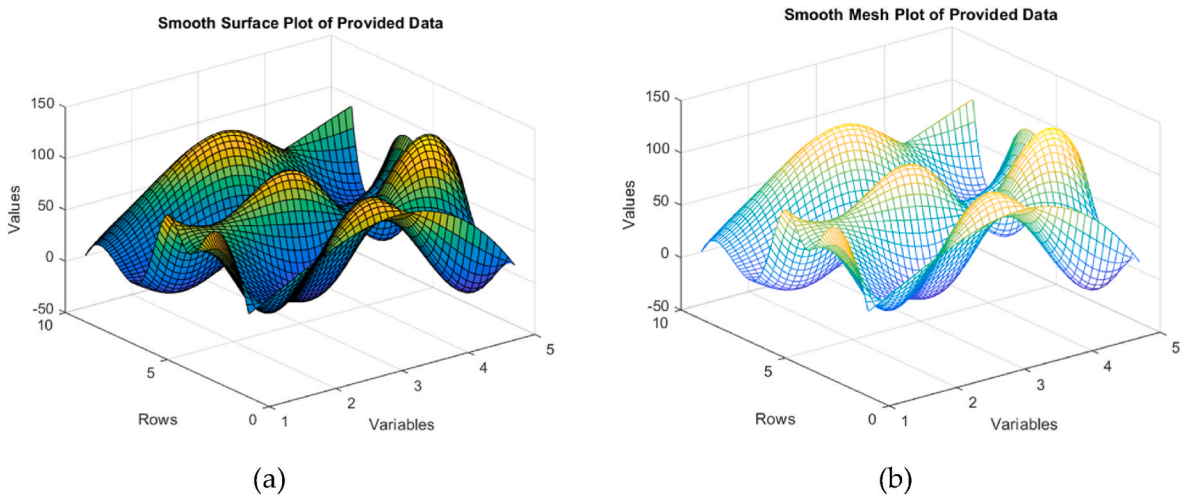

Fig. 8. Surface Representation of Interpolated Data in XGBoost model.

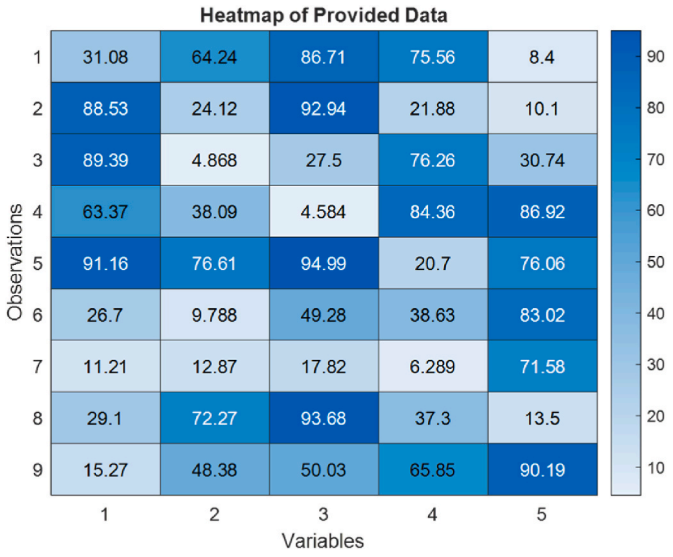

Fig. 9. Heatmap plot in the distribution of values in dataset.

variations across observations. The heatmap can provide insights into how the values in the data are distributed and can help identify any clusters or trends that might exist.

The present study offers a concise and noteworthy overview of diverse anti-infection strategies employed by various medicinal nanoparticles, including zinc oxide. The need for harmful chemicals as reducing and capping agents in nanoparticle synthesis from plant sources is eliminated, rendering the process both cost-effective and environmentally beneficial. Nanomedicine has demonstrated enhanced ability to infiltrate epithelial cells and inflammatory cells, thus augmenting treatment efficiency and longevity through precise targeting. Additionally, nanoparticles synthesized using green methods exhibit heightened efficacy against inflammation compared to traditionally synthesized counterparts. This research briefly delves into interactions between nanomedicines and their anti-inflammatory impact on cells, as well as common mechanisms underlying anti-inflammatory activity. Furthermore, the synthesis of herbal nanoparticles and nanoemulsions is touched upon in this study.

4. Conclusion

Children often suffer from otitis media with effusion, which may develop into cholesteatomata's chronic otitis if not treated. Consultation-based diagnosis (through otoscopy) is straightforward. Assessment of hearing loss is necessary both before and after therapy. Even though pharmaceutical treatments may alleviate symptoms in the short term, they are not recommended for OME due to their lack of long-term efficacy (especially in terms of the auditory threshold), their related side effects, and their expense. WAI has been developed to verify the wideband acoustic transferring performance of the middle ear over a comprehensive f level from 0.22 to 8.5 kHz. The OME samples (n = 60) and control group (n = 30) (1–10 years) have also been tested in WAI. Before surgically implanting tympanostomy tubes, wideband acoustic immittance testing was performed on kids with OME in the kids' pre-operative waiting area. All ears were tested using wideband tympanometry in a pressured environment, and some ears were also tested under ambient conditions. The surgeons reported their intraoperative findings on the amount of the outflow just before the tube installation, and this was verified after myringotomy. The degree of effusion can be classified as complete, partial, or absent, depending on its correlation with the middle ear volume. The categorization of absorbance responses into full, partial, and effusion-free at the time of surgery and standard control groups was based on the measurement of effusion volume. All individuals in the study population also underwent a standardized tympanometry test. As the quantity of middle ear effusion increased, there was a corresponding reduction in absorption. The f ranges from 1 to 5 kHz showed the highest absorption, while it was presented at all frequencies. The ears were classified into two categories: those with effusion present (including full and partial ears) and those without effusion (including clear ears and normal control ears). Ears with effusion were put into two groups: those with partial flow and those with full effusion. Ears without effusion were put into two groups: those with normal control ears and those with ears free of effusion. Overall, this method was very good at determining if an ear had flow and, if it did, how much effusion it had. The areas under the curve ranged from 1 to 0.970. Even though neither a normal control nor a clear ear had flow, this test could tell the difference among the two types of ears with some specificity and sensitivity. No statistically significant correlation among effusion volume and standard tympanometry was observed. In children with OME, WAI and, more significantly, absorption was robust and sensitive indication of middle ear effusion volume. In this study, by harnessing XGBoost, the RMSE of 1.223 units, R^2 of 0.899, and the ROC AUC of 0.944 signifies robust discrimination power. These pivotal metrics collectively underscore the model's accuracy, predictive capability, and discriminatory strength, affirming its potential as a reliable diagnostic tool for Wideband Absorbance Immittance (WAI) measurements. These methods face limitations such as inadequate drug-delivery

to the target site, potential inner-ear damage, and limited patient compliance, highlighting the need for improved approaches. Nanoparticle-based delivery methods for inner-ear diseases, including inorganic nanoparticles (silica, gold, iron oxide) and soft materials (liposomes, hydrogels), show potential in regulating drug administration, enhancing cell targeting, and decreasing systemic adverse effects. These nanoparticles can be designed for controlled drug release and functionalized for specific inner-ear cell receptors, improving drug uptake by target cells. Delivering drugs directly to the inner-ear minimizes systemic exposure, offering a promising approach for more effective and targeted treatments for hearing loss and vestibular disorders.

Credit author statement

In the intricate tapestry of scientific research, every thread, no matter how small, plays a pivotal role. Our recent exploration into the realm of inner ear treatment, emphasizing nanoparticles and predictive analytics, is no exception. This endeavor was the culmination of diverse expertise, tireless commitment, and collaborative synergy, as evidenced by the varied contributions of our team members.

Methodology: Prof. Zhang and Prof. Assilzadeh were instrumental in designing the methodology of the research. Their combined expertise ensured a rigorous and comprehensive approach. They scrutinized the potential of Zinc oxide nanoparticles for targeted drug delivery, ensuring a solid foundation for the study.

Data Curation and Analysis: Die Yu and Dr. Huang, with their keen analytical skills, played a pivotal role in curating the data from the Wideband Absorbance Immittance (WAI) measuring test. Dr. Chen1 further refined this dataset with meticulous formal analysis, transforming raw data into meaningful insights.

Validation: Under the guidance of Prof. Chen, the team embarked on the validation process. His vast experience and knack for detail provided the necessary rigor to our findings, establishing the efficiency of cochlear surgery in tandem with WAI.

Supervision, Project Administration, and Resources: Prof. Elkamchouchi was the beacon of guidance throughout the research. As a seasoned academic and researcher, he took on the mantle of supervision, ensuring the study maintained its intended direction and purpose. He also oversaw project administration, optimizing the allocation of resources, and ensuring a seamless execution of the research processes.

Application of Predictive Analytics: Dr. Alqahtani's expertise in predictive analytics was invaluable. By implementing the XGBoost model, he not only enhanced the depth of our research but also amplified its practical implications, paving the way for innovative treatments in the future.

Writing - Review & Editing: Prof. Huang, being the corresponding author, was at the helm of the writing process. With contributions from Dr. Chen1 and Die Yu in the initial drafts, the manuscript underwent rigorous review and editing. Prof. Chen and Prof. Elkamchouchi further enriched the content, ensuring clarity, coherence, and scientific rigor.

To conclude, the collaborative spirit and combined expertise of our team members were the driving forces behind this research. The outcome is not just a testament to our collective efforts but also a beacon for future endeavors in the domain of inner ear treatments.

Funding

This research was jointly supported by Key Program of Zhejiang Provincial Natural Science Foundation of China under Grant No: LZ22H130001 and by the National Natural Science Foundation of China under Grant No:82171146 , 82171144. Princess Nourah bint Abdulrahman University Researchers Supporting Project number (PNURSP2023R238), Princess Nourah bint Abdulrahman University, Riyadh, Saudi Arabia.

Declaration of competing interest

The authors declare that they have no known competing financial interests or personal relationships that could have appeared to influence the work reported in this paper.

Data availability

Data will be made available on request.

Acknowledgments

Princess Nourah bint Abdulrahman University Researchers Supporting Project number (PNURSP2023R238), Princess Nourah bint Abdulrahman University, Riyadh, Saudi Arabia. The authors extend their appreciation to the Deanship of Scientific Research at King Khalid University (KKU) for funding this research through the Research Group Program Under the Grant Number:(R.G.P.2/516/44).

References

Akbar, S., et al., 2017. Raphanus sativus mediated synthesis, characterization and biological evaluation of zinc oxide nanoparticles. Nanosci. Nanotechnol. Lett. 9 (12), 2005–2012.
AkÇA, A., et al., 2021. A comparative study of CO catalytic oxidation on the single vacancy and di-vacancy graphene supported single-atom iridium catalysts: a DFT analysis. Surface. Interfac. 25, 101293.
Al Sharabati, M., et al., 2021. Biodegradable Polymers and Their Nano-Composites for the Removal of Endocrine-Disrupting Chemicals (EDCs) from Wastewater: A Review, vol. 202. Environmental Research, 111694.
Armaghani, D.J., Mirzaei, F., Shariati, M., Trung, N.T., Shariati, M., Trnavac, D., 2020. Hybrid ANN-based techniques in predicting cohesion of sandy-soil combined with fiber. Geomech. Eng 20 (3), 191–205.
Arrieta, A., Singh, J., 2004. Management of recurrent and persistent acute otitis media: new options with familiar antibiotics. Pediatr. Infect. Dis. J. 23 (2), S115–S124.
Basavegowda, N., Patra, J.K., Baek, K.-H., 2020. Essential oils and mono/bi/tri-metallic nanocomposites as alternative sources of antimicrobial agents to combat multidrug-resistant pathogenic microorganisms: an overview. Molecules 25 (5), 1058.
Bhuyan, B., et al., 2018. Design of a photoactive bimetallic Cu-Au@ g-C3N4 catalyst for visible light driven hydroxylation of the benzene reaction through C–H activation. Eur. J. Inorg. Chem. 2018 (34), 3849–3858.
Buehler, M.J., Misra, A., 2019. Mechanical behavior of nanocomposites. MRS Bull. 44 (1), 19–24.
Cech, R.M., et al., 2022. Reducing overall herbicide use may reduce risks to humans but increase toxic loads to honeybees, earthworms and birds. Environ. Sci. Eur. 34 (1), 44.
Chahnasir, E.S., Zandi, Y., Shariati, M., Dehghani, E., Toghroli, A., Mohamad, E.T., Khorami, M., 2018. Application of support vector machine with firefly algorithm for investigation of the factors affecting the shear strength of angle shear connectors. Smart Struct. Syst. 22 (4), 413–424.Chicago.
Chaudhary, A., et al., 2019. Antimicrobial activity of zinc oxide nanoparticles synthesized from Aloe vera peel extract. SN Appl. Sci. 1, 1–9.
Chen, M., et al., 2020. Research progress of catalyst layer and interlayer interface structures in membrane electrode assembly (MEA) for proton exchange membrane fuel cell (PEMFC) system. ETransportation 5, 100075.
Csarnovics, I., et al., 2020. Development and study of biocompatible polyurethane-based polymer-metallic nanocomposites. Nanotechnol. Sci. Appl. 13, 11–22.
Cui, Y., Li, N., Misra, A., 2019. An overview of interface-dominated deformation mechanisms in metallic nanocomposites elucidated using in situ straining in a TEM. J. Mater. Res. 34 (9), 1469–1478.
Cui, Y., et al., 2022. Oral delivery of superoxide dismutase by lipid polymer hybrid nanoparticles for the treatment of ulcerative colitis. Chin. Chem. Lett. 33 (10), 4617–4622.
Danti, S., et al., 2020. Lithium niobate nanoparticles as biofunctional interface material for inner ear devices. Biointerphases 15 (3), 031004.
De Jong, W.H., Borm, P.J., 2008. Drug delivery and nanoparticles: applications and hazards. Int. J. Nanomed. 3 (2), 133.
Ensafi, A.A., Dadkhah-Tehrani, S., Karimi-Maleh, H., 2011. A voltammetric sensor for the simultaneous determination of l-cysteine and tryptophan using a p-aminophenol-multiwall carbon nanotube paste electrode. Anal. Sci. 27 (4), 409–414.
Gheorghe, D.C., et al., 2021. Nanoparticles for the treatment of inner ear infections. Nanomaterials 11 (5), 1311.
Gupta, A.S., 2011. Nanomedicine approaches in vascular disease: a review. Nanomed. Nanotechnol. Biol. Med. 7 (6), 763–779.
Heydari, A., Shariati, M., 2018. Buckling analysis of tapered BDFGM nano-beam under variable axial compression resting on elastic medium. Structural Engineering and Mechanics, An Int'l Journal 66 (6), 737–748.
Hojjati-Najafabadi, A., et al., 2021. A tramadol drug electrochemical sensor amplified by biosynthesized Au nanoparticle using mentha aquatic extract and ionic liquid. Top. Catal. 1–8.

Holzinger, M., Le Goff, A., Cosnier, S., 2014. Nanomaterials for biosensing applications: a review. Front. Chem. 2, 63.
Hosur Shivaramaiah, Kattimani, S., Shariati, M., Nguyen-Thoi, T., 2022. Geometrically nonlinear behavior of two-directional functionally graded porous plates with four different materials. Proc. Inst. Mech. Eng. J. Mech. Eng. Sci. 236 (22), 11008–11023.
Huang, H., et al., 2021. Electrochemical sensor based on Ce-MOF/carbon nanotube composite for the simultaneous discrimination of hydroquinone and catechol. J. Hazard Mater. 416, 125895.
Jahannoosh, M., et al., 2021. New hybrid meta-heuristic algorithm for reliable and cost-effective designing of photovoltaic/wind/fuel cell energy system considering load interruption probability. J. Clean. Prod. 278, 123406.
Joo, H., et al., 2020. Material design and fabrication strategies for stretchable metallic nanocomposites. Small 16 (11), 1906270.
Kamyab, H., Chelliapan, S., Hayder, G., Yusuf, M., Taheri, M.M., Rezania, S., Nouri, J., 2023. Exploring the potential of layered metal and metal oxide nanomaterials for sustainable water and wastewater treatment: A review of their antimicrobial properties. Chemosphere 139103. https://doi.org/10.1016/j.chemosphere.2023.139103.
Karaman, C., 2021. Orange peel derived-nitrogen and sulfur Co-doped carbon dots: a nano-booster for enhancing ORR electrocatalytic performance of 3D graphene networks. Electroanalysis 33 (5), 1356–1369.
Karimi, F., et al., 2022. Removal of metal ions using a new magnetic chitosan nano-bio-adsorbent; A powerful approach in water treatment. Environ. Res. 203, 111753.
Karimi-Maleh, H., et al., 2022. A green and sensitive guanine-based DNA biosensor for idarubicin anticancer monitoring in biological samples: a simple and fast strategy for control of health quality in chemotherapy procedure confirmed by docking investigation. Chemosphere 291, 132928.
Karimi-Maleh, H., et al., 2023. Calf thymus ds-DNA intercalation with pendimethalin herbicide at the surface of ZIF-8/Co/rGO/C3N4/ds-DNA/SPCE; A bio-sensing approach for pendimethalin quantification confirmed by molecular docking study. Chemosphere 332, 138815.
Kirschner, D., Lenhart, S., Serbin, S., 1997. Optimal control of the chemotherapy of HIV. J. Math. Biol. 35 (7), 775–792.
Klein, J. and S. Pelton, Epidemiology, Pathogenesis, Clinical Manifestations, and Complications of Acute Otitis Media. Accessed May 15, 2007.
Kontiokari, T., et al., 1998. Symptoms of acute otitis media. Pediatr. Infect. Dis. J. 17 (8), 676–679.
Korkmaz, S., et al., 2021. The production of rGO/RuO2 aerogel supercapacitor and analysis of its electrochemical performances. Ceram. Int. 47 (24), 34514–34520.
Lee, H.-S., et al., 2022. Pendimethalin induces apoptotic cell death through activating ER stress-mediated mitochondrial dysfunction in human umbilical vein endothelial cells. Food Chem. Toxicol. 168, 113370.
Li, K., Liu, B., 2014. Polymer-encapsulated organic nanoparticles for fluorescence and photoacoustic imaging. Chem. Soc. Rev. 43 (18), 6570–6597.
Li, J., et al., 2023. A New Formulation of Ni/Zn Bi-metallic Nanocomposite and Evaluation of its Applications for Pollution Removal, Photocatalytic, Electrochemical Sensing, and Anti-breast Cancer. Environmental Research, 116462.
Ly, N.H., Nguyen, N.B., Tran, H.N., Hoang, T.T.H., Joo, S.W., Vasseghian, Y., Klemeš, J. J., 2023. Metal-organic framework nanopesticide carrier for accurate pesticide delivery and decrement of groundwater pollution. J. Clean. Prod. 402, 136809. https://doi.org/10.1016/j.jclepro.2023.136809.
Mäder, K., et al., 2018. Controlled drug release to the inner ear: concepts, materials, mechanisms, and performance. Hear. Res. 368, 49–66.
Mariadoss, A.V.A., et al., 2020. Folic acid functionalized starch encapsulated green synthesized copper oxide nanoparticles for targeted drug delivery in breast cancer therapy. Int. J. Biol. Macromol. 164, 2073–2084.
Maslahati Roudi, A., et al., 2018. Prediction and optimization of the fenton process for the treatment of landfill leachate using an artificial neural network. Water 10 (5), 595.
McCall, A.A., et al., 2010. Drug delivery for treatment of inner ear disease: current state of knowledge. Ear Hear. 31 (2), 156.
McNamara, K., Tofail, S.A., 2015. Nanosystems: the use of nanoalloys, metallic, bimetallic, and magnetic nanoparticles in biomedical applications. Phys. Chem. Chem. Phys. 17 (42), 27981–27995.
Medetalibeyoğlu, H., et al., 2020. Molecular imprinted sensor including Au nanoparticles/polyoxometalate/two-dimensional hexagonal boron nitride nanocomposite for diazinon recognition. ECS J. Solid State Sci. Technol. 9 (10), 101006.
Moghaddam, F.D., et al., 2022. Carbohydrate Polymer-Based Nanocomposites for Breast Cancer Treatment. Carbohydrate Polymers, 120510.
Mohammadhassani, M., Nezamabadi-Pour, H., Suhatril, M., Shariati, M., 2013. Identification of a suitable ANN architecture in predicting strain in tie section of concrete deep beams. Structural Engineering and Mechanics, An Int'l Journal 46 (6), 853–868.Chicago.
Mohammadhassani, M., Nezamabadi-Pour, H., Suhatril, M., Shariati, M., 2014. An evolutionary fuzzy modelling approach and comparison of different methods for shear strength prediction of high-strength concrete beams without stirrups. Smart Struct. Syst. Int. J. 14 (5), 785–809.
Moruskar, A.S., et al., 2023. Nanocrystalline silver for the treatment of otomycosis: a retrospective study. Iran J Otorhinolaryngol 35 (127), 83–89.
Nguyen, K., et al., 2017. Recent advances in therapeutics and drug delivery for the treatment of inner ear diseases: a patent review (2011-2015). Expert Opin. Ther. Pat. 27 (2), 191–202.
Niemela, M., et al., 1994. Lack of specific symptomatology in children with acute otitis media. Pediatr. Infect. Dis. J. 13 (9), 765–768.
Özcan, N., et al., 2020. A novel molecularly imprinting biosensor including graphene quantum dots/multi-walled carbon nanotubes composite for interleukin-6 detection and electrochemical biosensor validation. ECS J. Solid State Sci. Technol. 9 (12), 121010.
Oliveira Jr., O.N., et al., 2014. Nanomaterials for diagnosis: challenges and applications in smart devices based on molecular recognition. ACS Appl. Mater. Interfaces 6 (17), 14745–14766.
Omanović-Mikličanin, E., et al., 2020. Nanocomposites: A brief review. Health and Technology (10), 51–59.
Praetorius, M., et al., 2007. Transsynaptic delivery of nanoparticles to the central auditory nervous system. Acta Otolaryngol. 127 (5), 486–490.
Qiao, J., Li, X., Qi, L., 2022. Fluorescent polymer-modified gold nanobipyramids for temperature sensing during photothermal therapy in living cells. Chin. Chem. Lett. 33 (6), 3193–3196.
Rajkumar, V., Guha, G., Kumar, R.A., 2012. Isolation and bioactivity evaluation of two metabolites from the methanolic extract of Oroxylum indicum stem bark. Asian Pac. J. Trop. Biomed. 2 (1), S7–S11.
Raoof, J.B., Ojani, R., Karimi-Maleh, H., 2009. Electrocatalytic oxidation of glutathione at carbon paste electrode modified with 2,7-bis (ferrocenyl ethyl) fluoren-9-one: application as a voltammetric sensor. J. Appl. Electrochem. 39 (8), 1169–1175.
Rasouli, K., Rasouli, J., Mohtaram, M.S., Sabbaghi, S., Kamyab, H., Moradi, H., Chelliapan, S., 2023. Biomass-derived activated carbon nanocomposites for cleaner production: A review on aspects of photocatalytic pollutant degradation. J. Clean. Prod. 138181. https://doi.org/10.1016/j.jclepro.2023.138181.
Ren, Y., Landegger, L.D., Stankovic, K.M., 2019. Gene therapy for human sensorineural hearing loss. Front. Cell. Neurosci. 13, 323.
Rohit, J.V., Kailasa, S.K., 2017. Simple and selective detection of pendimethalin herbicide in water and food samples based on the aggregation of ractopamine-dithiocarbamate functionalized gold nanoparticles. Sensor. Actuator. B Chem. 245, 541–550.
Ross, A.M., et al., 2016. Persistence, distribution, and impact of distinctly segmented microparticles on cochlear health following in vivo infusion. J. Biomed. Mater. Res. 104 (6), 1510–1522.
Rothman, R., Owens, T., Simel, D.L., 2003. Does this child have acute otitis media? JAMA 290 (12), 1633–1640.
Safa, M., Kachitvichyanukul, V., 2019. Moment rotation prediction of precast beam to column connections using extreme learning machine. Structural Engineering and Mechanics, An Int'l Journal 70 (5), 639–647.
Safa, M., Sari, P.A., Shariati, M., Suhatril, M., Trung, N.T., Wakil, K., Khorami, M., 2020. Development of neuro-fuzzy and neuro-bee predictive models for prediction of the safety factor of eco-protection slopes. Physica A: Stat. Mech. Appl. 550, 124046.
Safa, M., Shariati, M., Ibrahim, Z., Toghroli, A., Baharom, S.B., Nor, N.M., Petković, D., 2016. Potential of adaptive neuro fuzzy inference system for evaluating the factors affecting steel-concrete composite beam's shear strength. *Steel and Composite Structures*. Int. J. 21 (3), 679–688.
Sajedi, F., Shariati, M., 2019. Behavior study of NC and HSC RCCs confined by GRP casing and CFRP wrapping. Steel Compos. Struct 30 (5), 417–432.
Sajjadian, S.M., Jafari, M., Chen, X., 2022. Automatic Architectural Drawing Labelling Using Deep Convolutional Neural Network. In: *Sustainability in Energy and Buildings 2021*. Springer, Singapore, pp. 69–78.
Sajjadian, S.M., Jafari, M., Pekaslan, D., 2020. An expandable, contextualized and data-driven indoor thermal comfort model. Energy Built Environ. 1 (4), 385–392.
Salem, W., et al., 2015. Antibacterial activity of silver and zinc nanoparticles against Vibrio cholerae and enterotoxic Escherichia coli. Int. J. Med. Microbiol. 305 (1), 85–95.
Schilder, A.G., et al., 2019. Hearing protection, restoration, and regeneration: an overview of emerging therapeutics for inner ear and central hearing disorders. Otol. Neurotol. 40 (5), 559–570.
Sedghi, Y., Zandi, Y., Shariati, M., Ahmadi, E., Azar, V.M., Toghroli, A., Wakil, K., 2018. Application of ANFIS technique on performance of C and L shaped angle shear connectors. Smart struct. Syst. 22 (3), 335–340.
Shahnazi, A., Nabid, M.R., Sedghi, R., 2020. Synthesis of surface molecularly imprinted poly-o-phenylenediamine/TiO2/carbon nanodots with a highly enhanced selective photocatalytic degradation of pendimethalin herbicide under visible light. React. Funct. Polym. 151, 104580.
Shariati, M., Davoodnabi, S.M., Toghroli, A., Kong, Z., Shariati, A., 2021. Hybridization of metaheuristic algorithms with adaptive neuro-fuzzy inference system to predict load-slip behavior of angle shear connectors at elevated temperatures. Compos. Struct. 278, 114524.
Shariati, M., Kamyab, H., Habibi, M., Ahmadi, S., Naghipour, M., Gorjinezhad, F., Aminian, A., 2023. Sulfuric acid resistance of concrete containing coal waste as a partial substitute for fine and coarse aggregates. Fuel 348, 128311.
Shariati, Mahdi et al. Assessment of Longstanding Effects of Fly Ash and Silica Fume on the Compressive Strength of Concrete Using Extreme Learning Machine and Artificial Neural Network. J. Adv. Eng. Comput., [S.l.], v. 5, n. 1, p. 50-74, mar. 2021. doi: http://dx.doi.org/10.25073/jaec.202151.308.
Shariati, M., Mafipour, M.S., Haido, J.H., Yousif, S.T., Toghroli, A., Trung, N.T., Shariati, A., 2020. Identification of the most influencing parameters on the properties of corroded concrete beams using an Adaptive Neuro-Fuzzy Inference System (ANFIS). Steel Compos. Struct. 34 (1), 155.
Shariati, M., Mafipour, M.S., Mehrabi, P., Ahmadi, M., Wakil, K., Trung, N.T., Toghroli, A., 2020. Prediction of concrete strength in presence of furnace slag and fly ash using Hybrid ANN-GA (Artificial Neural Network-Genetic Algorithm). Smart Struct. Syst. Int. J. 25 (2), 183–195.
Shariati, M., Mafipour, M.S., Mehrabi, P., Bahadori, A., Zandi, Y., Salih, M.N., Poi-Ngian, S., 2019. Application of a hybrid artificial neural network-particle swarm

optimization (ANN-PSO) model in behavior prediction of channel shear connectors embedded in normal and high-strength concrete. Appl. Sci. 9 (24), 5534.
Shariati, M., Mafipour, M.S., Mehrabi, P., Shariati, A., Toghroli, A., Trung, N.T., Salih, M. N., 2021. A novel approach to predict shear strength of tilted angle connectors using artificial intelligence techniques. *Engineering with*. Computers 37, 2089–2109.
Shariati, M., Mafipour, M.S., Mehrabi, P., Zandi, Y., Dehghani, D., Bahadori, A., Poi-Ngian, S., 2019. Application of Extreme Learning Machine (ELM) and Genetic Programming (GP) to design steel-concrete composite floor systems at elevated temperatures. Steel Compos. Struct 33 (3), 319–332.
Shariati, M., Mafipour, M.S., Ghahremani, B., Azarhomayun, F., Ahmadi, M., Trung, N. T., Shariati, A., 2022. A novel hybrid extreme learning machine–grey wolf optimizer (ELM-GWO) model to predict compressive strength of concrete with partial replacements for cement. Eng. Comput. 1–23.
Shu, L., et al., 2021. Assessment methodology applied to arsenic pollution in lake sediments combining static and dynamic processes. Chemosphere 277, 130260.
Sun, C.-Y., et al., 2019. Phytochemicals: current strategy to sensitize cancer cells to cisplatin. Biomed. Pharmacother. 110, 518–527.
Tahernejad-Javazmi, F., Shabani-Nooshabadi, M., Karimi-Maleh, H., 2018. Gold nanoparticles and reduced graphene oxide-amplified label-free DNA biosensor for dasatinib detection. New J. Chem. 42 (19), 16378–16383.
Tajuddeen, I., Sajjadian, S.M., Jafari, M., 2023. Regression models for predicting the global warming potential of thermal insulation materials. Buildings 13 (1), 171.
Tavakkoli, O., Kamyab, H., Shariati, M., Mohamed, A.M., Junin, R., 2022. Effect of nanoparticles on the performance of polymer/surfactant flooding for enhanced oil recovery: A review. Fuel 312, 122867.
Toghroli, A., Mohammadhassani, M., Suhatril, M., Shariati, M., Ibrahim, Z., 2014. Prediction of shear capacity of channel shear connectors using the ANFIS model. Steel Compos. Struct 17 (5), 623–639.
Traverso, N., et al., 2013. Role of glutathione in cancer progression and chemoresistance. Oxid. Med. Cell. Longev. 2013.
Trichopoulos, D., MacMahon, B., Cole, P., 1972. Menopause and breast cancer Risk2. J. Natl. Cancer Inst.: J. Natl. Cancer Inst. 48 (3), 605–613.
Vigano, L., et al., 2018. Use of chlorhexidine, side effects and antibiotic resistance. Biointerface Res. Applied Chem. 8 (3), 3265–3266.
Wang, H., et al., 2021. Update on nanoparticle-based drug delivery system for anti-inflammatory treatment. Front. Bioeng. Biotechnol. 9, 630352.
Wang, Z., et al., 2022. Visualized uranium rapid monitoring system based on self-enhanced electrochemiluminescence-imaging of amidoxime functionalized polymer nanoparticles. Chin. Chem. Lett. 33 (7), 3456–3460.
Won, J., et al., 2020. Assessing the effect of middle ear effusions on wideband acoustic immittance using optical coherence tomography. Ear Hear. 41 (4), 811.
Xing, C., et al., 2018. Conceptually novel black phosphorus/cellulose hydrogels as promising photothermal agents for effective cancer therapy. Adv. Healthcare Mater. 7 (7), 1701510.
Xu, Y., et al., 2022. Two-dimensional coordination polymer-based nanosensor for sensitive and reliable nucleic acids detection in living cells. Chin. Chem. Lett. 33 (2), 968–972.
Yazdani, M., Kabirifar, K., Frimpong, B.E., Shariati, M., Mirmozaffari, M., Boskabadi, A., 2021. Improving construction and demolition waste collection service in an urban area using a simheuristic approach: A case study in Sydney, Australia. J. Clean. Prod. 280, 124138. Chicago.
Zhang, Z., et al., 2021a. Drug delivery across barriers to the middle and inner ear. Adv. Funct. Mater. 31 (44), 2008701.
Zhang, T., et al., 2021b. Zwitterionic comb-like lipid polymers encapsulating linalool for increasing the fragrance retention time. Chin. Chem. Lett. 32 (1), 573–576.